



# Profiling Basal Forebrain Cholinergic Neurons Reveals a Molecular Basis for Vulnerability Within the Ts65Dn Model of Down Syndrome and Alzheimer's Disease

Melissa J. Alldred<sup>1,3</sup> · Sai C. Penikalapati<sup>1</sup> · Sang Han Lee<sup>2</sup> · Adriana Heguy<sup>4</sup> · Panos Roussos<sup>1,5</sup> · Stephen D. Ginsberg<sup>1,3,6,7</sup>

Received: 29 December 2020 / Accepted: 13 June 2021 / Published online: 14 July 2021

© The Author(s), under exclusive licence to Springer Science+Business Media, LLC, part of Springer Nature 2021

## Abstract

Basal forebrain cholinergic neuron (BFCN) degeneration is a hallmark of Down syndrome (DS) and Alzheimer's disease (AD). Current therapeutics have been unsuccessful in slowing disease progression, likely due to complex pathological interactions and dysregulated pathways that are poorly understood. The Ts65Dn trisomic mouse model recapitulates both cognitive and morphological deficits of DS and AD, including BFCN degeneration. We utilized Ts65Dn mice to understand mechanisms underlying BFCN degeneration to identify novel targets for therapeutic intervention. We performed high-throughput, single population RNA sequencing (RNA-seq) to interrogate transcriptomic changes within medial septal nucleus (MSN) BFCNs, using laser capture microdissection to individually isolate ~500 choline acetyltransferase-immunopositive neurons in Ts65Dn and normal disomic (2N) mice at 6 months of age (MO). Ts65Dn mice had unique MSN BFCN transcriptomic profiles at ~6 MO clearly differentiating them from 2N mice. Leveraging Ingenuity Pathway Analysis and KEGG analysis, we linked differentially expressed gene (DEG) changes within MSN BFCNs to several canonical pathways and aberrant physiological functions. The dysregulated transcriptomic profile of trisomic BFCNs provides key information underscoring selective vulnerability within the septohippocampal circuit. We propose both expected and novel therapeutic targets for DS and AD, including specific DEGs within cholinergic, glutamatergic, GABAergic, and neurotrophin pathways, as well as select targets for repairing oxidative phosphorylation status in neurons. We demonstrate and validate this interrogative quantitative bioinformatic analysis of a key dysregulated neuronal population linking single population transcript changes to an established pathological hallmark associated with cognitive decline for therapeutic development in human DS and AD.

**Keywords** RNA-seq · Medial septum · Down syndrome · Alzheimer's disease · Selective vulnerability · Bioinformatics

✉ Stephen D. Ginsberg  
ginsberg@nki.rfmh.org

Melissa J. Alldred  
Melissa.Allred@nki.rfmh.org

Sai C. Penikalapati  
penikalapati.s@northeastern.edu

Sang Han Lee  
SangHan.Lee@nki.rfmh.org

Adriana Heguy  
Adriana.Heguy@nyulangone.org

Panos Roussos  
Panagiotis.Roussos@nki.rfmh.org

<sup>2</sup> Center for Biomedical Imaging and Neuromodulation, Nathan Kline Institute, Orangeburg, NY, USA

<sup>3</sup> Departments of Psychiatry, New York University Grossman School of Medicine, New York, NY, USA

<sup>4</sup> Genome Technology Center, New York University Grossman School of Medicine, New York, NY, USA

<sup>5</sup> Departments of Genetics and Genomic Sciences and Psychiatry and the Institute for Data Science and Genomic Technology, Icahn School of Medicine at Mount Sinai, New York, NY, USA

<sup>6</sup> Neuroscience & Physiology, New York University Grossman School of Medicine, New York, NY, USA

<sup>1</sup> Center for Dementia Research, Nathan Kline Institute, 140 Old Orangeburg Road, Orangeburg, NY 10962, USA

<sup>7</sup> NYU Neuroscience Institute, New York University Grossman School of Medicine, New York, NY, USA

## Background

Down syndrome (DS) is caused by triplication of human chromosome 21 (HSA21), observed in ~1 of 700 births [1]. Estimates indicate >250,000 persons with DS live in the USA [2]. DS is the primary genetic cause of intellectual disability and results in a number of neurological conditions, including deficits in learning and memory [3–8]. Individuals with DS also show age-dependent neurodegeneration early in mid-life associated with Alzheimer's disease (AD), including amyloid plaques, neurofibrillary tangles, and dementia in ~70% of individuals [9–15]. In both AD and DS, age-related cognitive decline is associated with degeneration of the cholinergic basal forebrain system, including loss of cholinergic basal forebrain neurons in the nucleus basalis and cholinergic fiber projections to the hippocampus and neocortex [4, 16–18].

The Ts65Dn mouse model recapitulates many human DS neuropathological endophenotypes including AD-like hippocampal-dependent learning and memory deficits, basal forebrain cholinergic neuron (BFCN) degeneration and septohippocampal circuit dysfunction, notably CA1 pyramidal neuron and choline acetyltransferase (ChAT) activity deficits [9, 19–23]. Interrogating memory requires a complex paradigm that involves multiple circuits in the brain, including memory consolidation in the locus coeruleus [24, 25], serotonergic neurons of the median raphe nucleus which affect memory formation [26], medial prefrontal cortex pyramidal neurons [27], and cholinergic projection systems emanating from the basal forebrain [28], which interact with and/or innervate the hippocampus and cortical mantle. While cognitive decline in DS is associated with degeneration of the BFCN projection system, the medial septal/ventral diagonal band, which projects to the hippocampus, is critical for multiple classifications of memory [22, 23, 29–34]. Degeneration in this projection system is a cardinal feature of the Ts65Dn mouse [21, 23, 31, 35–40]. BFCN changes begin approximately at 6 months of age (MO) [21, 31, 32, 41]. BFCN loss and changes in hippocampal innervation are consistently reported in Ts65Dn mice >10 MO [31, 32, 34, 42, 43]. Expression level changes in trisomic mice have been limited to regional analysis [42, 44] or specific neuronal subtype assessment by microarrays [40, 45–49].

Prior to RNA sequencing (RNA-seq) technologies, researchers queried RNA expression levels using qRT-PCR, microarray analysis, and chip-based technologies [50–58]. While these methods show high overlap with RNA-seq results [59], they have drawbacks, including the number of genes queried, cost effectiveness, input quantity, and sequence specificity [60, 61]. RNA-seq has several key benefits, including identification of noncoding RNA (ncRNA) species, sequence variations, including single-nucleotide polymorphisms and highly homologous sequences, with virtually no background

[62]. Additionally, cost versus sequencing depth has been greatly reduced. RNA-seq advanced concomitantly with the ability to isolate individual cells through laser capture microdissection (LCM), microfluidics, and flow cytometry [63–66].

This study employs LCM and single population RNA-seq to profile vulnerable BFCNs, an approach that has decided advantages over regional-based tactics. We postulate by isolating vulnerable ChAT-immunopositive BFCNs from heterogenous medial septal nucleus (MSN) populations and identifying dysregulated genes. We will identify cell type-specific therapeutic targets that may help slow or stop the progression of BFCN degeneration associated with AD and DS. We hypothesize differentially expressed gene (DEG) changes are not solely due to the triplicated “DS gene region” and involve novel pathways and targets that have not been previously identified or considered causative of BFCN dysfunction.

## Methods

### Mice

Animal protocols were approved by the Nathan Kline Institute/NYU Grossman School of Medicine IACUC in accordance with NIH guidelines. Breeder pairs (female Ts65Dn and male C57Bl/6 J Eicher × C3H/HeSnJ F1 mice) were purchased from Jackson Laboratories (Bar Harbor, ME, USA) and mated at the Nathan Kline Institute. Mice were kept on a standard chow diet with *ad libitum* water access [47, 48]. Mice were genotyped [67] at weaning and aged to ~6 MO.

### Tissue Preparation

Brain tissues were accessed from Ts65Dn (Ts;  $n = 6$ ) and normal disomic littermates (2N;  $n = 6$ ) male mice (age range, 5.8–6.4 MO; mean age, 6.0 MO). Mice were perfused transcardially with 0.15 M phosphate buffer as previously described [45, 47–49]. Brains were immediately flash frozen and 20- $\mu\text{m}$ -thick tissue sections were cryostat cut in the coronal plane (CM1860UV, Leica, Buffalo Grove, IL, USA) and mounted on polyethylene naphthalate (PEN) membrane slides (Leica) (Fig. 1B). Slides were kept under desiccant at  $-80\text{ }^{\circ}\text{C}$  until used for immunohistochemistry. RNase-free precautions were employed, and solutions were made with 18.2 mega Ohm RNase-free water (Nanopure Diamond, Barnstead, Dubuque, IA, USA).

### Immunohistochemistry

PEN membrane slides were equilibrated to room temperature (RT) under desiccant ( $-20\text{ }^{\circ}\text{C}$  for 5 min,  $4\text{ }^{\circ}\text{C}$  for 10 min, RT for 5 min) prior to staining (Fig. 1B–C). A quick staining protocol (<1 h) was utilized for RNA preservation in unfixed

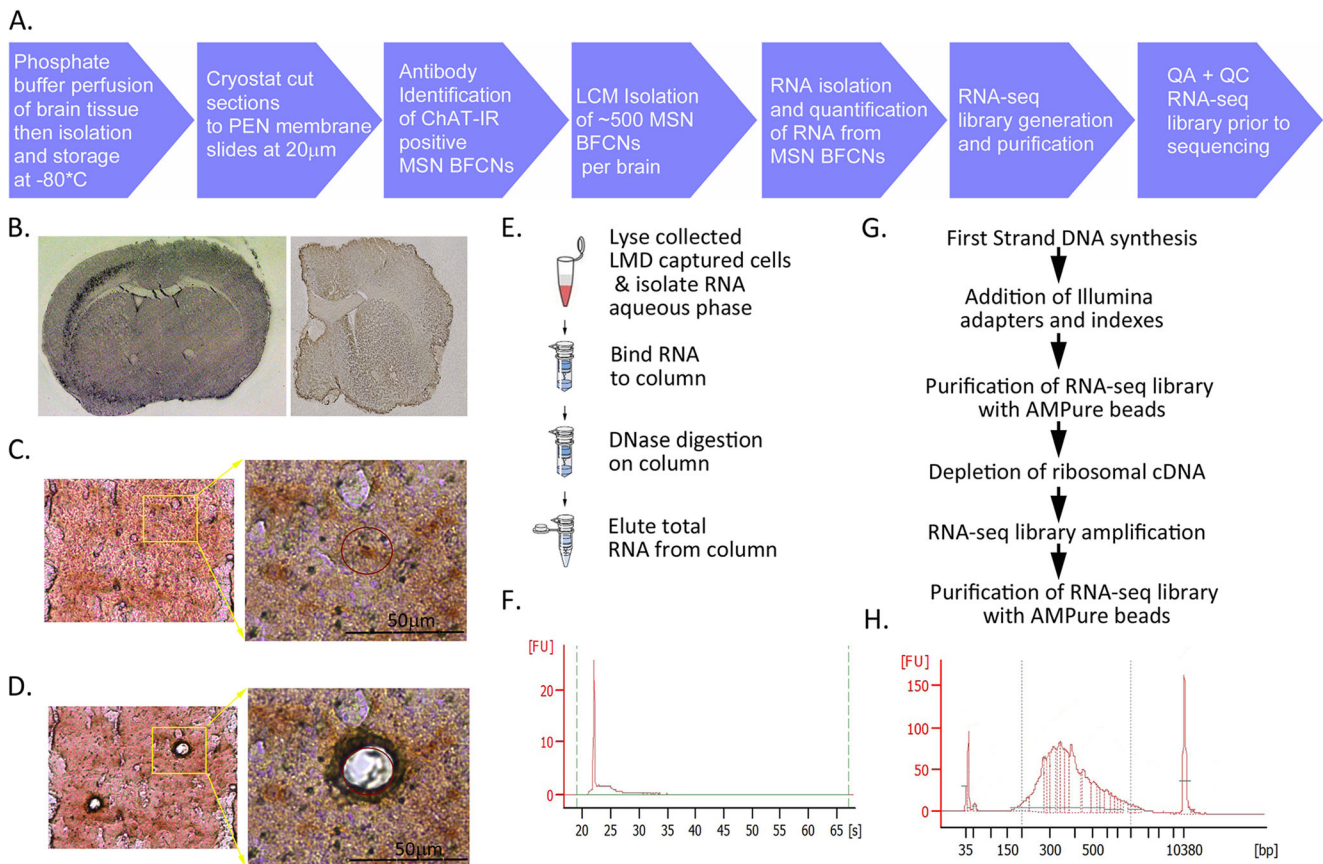


**Fig. 1** Overview of experimental workflow. **A** Flow chart illustrates isolation of MSN BFCNs, followed by RNA-seq library preparation. **B** Whole (left) or biased-hemibrains (cut biased to the midline by  $\sim 1\text{--}2$  mm to include entire MSN/VDB region; right) were cryocut at  $20\text{-}\mu\text{m}$  thickness and mounted on PEN membrane slides. **C** ChAT-immunopositive neurons were visualized at  $10\times$  and selected for isolation by LCM at  $40\times$ . **D** LCM was used to isolate neurons and tissue was checked for complete

cutting of each cell and collection via gravity into tubes containing lysis reagent. **E** RNA was isolated using the miRNeasy micro kit (Qiagen). **F** RNA quantity was determined (Agilent RNA 6000 Pico). **G.** RNA-seq library prep was performed using isolated RNA from LCM-captured MSN BFCNs (Takara). **H** RNA-seq library QC was performed for each sample (Agilent)

tissue. Slides were rinsed in phosphate-buffered saline (PBS, pH 7.4), blocked for 3 min in 2.5% normal horse serum. Primary antibody against ChAT (AB144P, Millipore; 1:50 dilution) in 2.5% normal horse serum with 20 U/ml of Superase-In RNase inhibitor (Ambion, ThermoFisher Scientific, Waltham, MA, USA) was incubated for 25 min at RT, with  $3\times$  PBS washes after each subsequent step. Secondary antibody (ImmPRESS Polymer Reagent, Vector Labs, Burlingame, CA, USA) was incubated on slides for 20 min, and incubated for 3–5 min in peroxidase substrate solution (ImmPACT NovaRED, Vector Labs). Slides were air-dried prior to LCM or re-frozen at  $-80^{\circ}\text{C}$  under desiccant.

## LCM

LMD7000 (Leica) was employed to identify individual ChAT-immunoreactive MSN/VDB (herein called MSN) BFCNs using a  $40\times$  objective (PL-Fluotar NA 0.60) and positive neurons were outlined using the draw/cut tool (Leica LMD version 8.0). Identified cells dropped by gravity into

$50\ \mu\text{l}$  Qiazol solution (Qiagen, Germantown, MD, USA) (Fig. 1C–D). Captured cells were counted and lysed cells were frozen until  $\sim 500$  cells/brain/region were isolated for RNA-seq analysis. On average 17 sections were needed to collect  $\sim 500$  ChAT-immunoreactive BFCNs for RNA-seq.

## RNA Purification

RNA from  $\sim 500$  BFCNs was purified using miRNeasy Micro kit (Qiagen) according to manufacturers' specifications. A DNase digestion was performed twice sequentially before the final washes and RNA purification (Fig. 1E). RNA quality control (QC) was performed (RNA 6000 pico kit, Agilent, Santa Clara, CA, USA; Fig. 1F).

## Library Preparation and RNA-seq

The SMARTer Stranded Total RNA-Seq Kit (Takara Bio, Mountain View, CA, USA; Fig. 1G) was employed with minor modifications to utilize full volume of RNA. Samples

were quantified (Agilent 2100 HS DNA kit; Fig. 1H), and samples below 2 nM of library were excluded. Samples were pooled in equimolar concentrations and assayed on an Illumina HiSeq-4000 (San Diego, CA, USA) using a single-read 50-cycle protocol at the Genome Technology Center, NYU Grossman School of Medicine.

## Bioinformatics

FastQ files were generated and QC of the raw reads were performed by Fastqc version 0.11.8 [68]. Read trimming was performed as necessary by Trimmomatic 0.39 [69]. If QC passed and showed no adapter contamination, this step was skipped. Sequence reads were aligned to the reference genome (Gencode GRCm38-mm10) using STAR Aligner (2.7.0) [70]. QC was performed on alignments using Rseqc (v3.0.0) and Picard (2.20.03) [71]. Pseudo alignment and read quantification was performed by Kallisto version 0.44.0 [72] using mouse reference genome (Gencode GRCm38-mm10).

## Statistical Analysis

Sample by gene count matrix obtained from Kallisto were further normalized using voom transformation [72, 73]. Genes with at least 2 counts per million (CPM) in 50% of samples were employed for downstream analysis. The normalized gene expression matrix was used to select known covariates. RNA concentration was used as a covariate and quality weights were obtained. The weighted multiple linear model was fit for each gene and contrasts were computed with Limma [74]. Gene expression differences at ( $p < 0.05$ ) were considered statistically significant. Protein coding genes were extracted using the R Bioconductor package AnnotationDbi [75]. Multiple testing corrections were performed by false discovery rate (FDR) [76].

## Pathway Analysis

Pathway analyses included Ingenuity Pathway Analysis (IPA; Qiagen) [77, 78], Kyoto Encyclopedia of Genes and Genomes (KEGG) [79], and STRING [80] in Cytoscape (cutoff 0.4) [81].

## qRT-PCR Validation

To preserve RNA quality to perform qRT-PCR analysis, a shorter staining protocol was employed. MSN neurons were isolated via LCM from adjacent tissue sections in the same animals as utilized for RNA-seq ( $n = 6$  per genotype) after Nissl-staining {0.1% thionin in sodium acetate (49.44 mM)/acetic acid (3.6 mM) buffer}. LCM was performed on Nissl-positive MSN neurons based on morphology, enriching for BFCNs. Approximately 200 neurons/sample were collected

based on manufacturer's recommendation and empirical assessments (TaqMan Gene Expression Cell to Ct kit, ThermoFisher). qPCR was performed utilizing 2  $\mu$ l cDNA, from 50  $\mu$ l reaction with 22.5  $\mu$ l input RNA. Taqman qPCR primers (Life Technologies, Grand Island, NY, USA) for 11 genes were selected for specific gene candidates from significantly affected pathways from IPA and KEGG analysis (Supplemental Table 1) to assay samples in triplicate on a real-time PCR cycler (PikoReal, ThermoFisher). The ddCT method was used to determine relative gene level differences between groups [82–84]. Glucuronidase beta (*Gusb*) PCR products were utilized as a control, as *Gusb* did not show significant changes in RNA-seq data obtained from BFCNs. Negative controls consisted of the reaction mixture without input RNA. The two study groups (Ts and 2N) were compared with respect to PCR product synthesis for each gene tested. qRT-PCR log-fold change (LFC) were scored without significance measures due to low expression and variability from the cell to CT protocol.

## Results

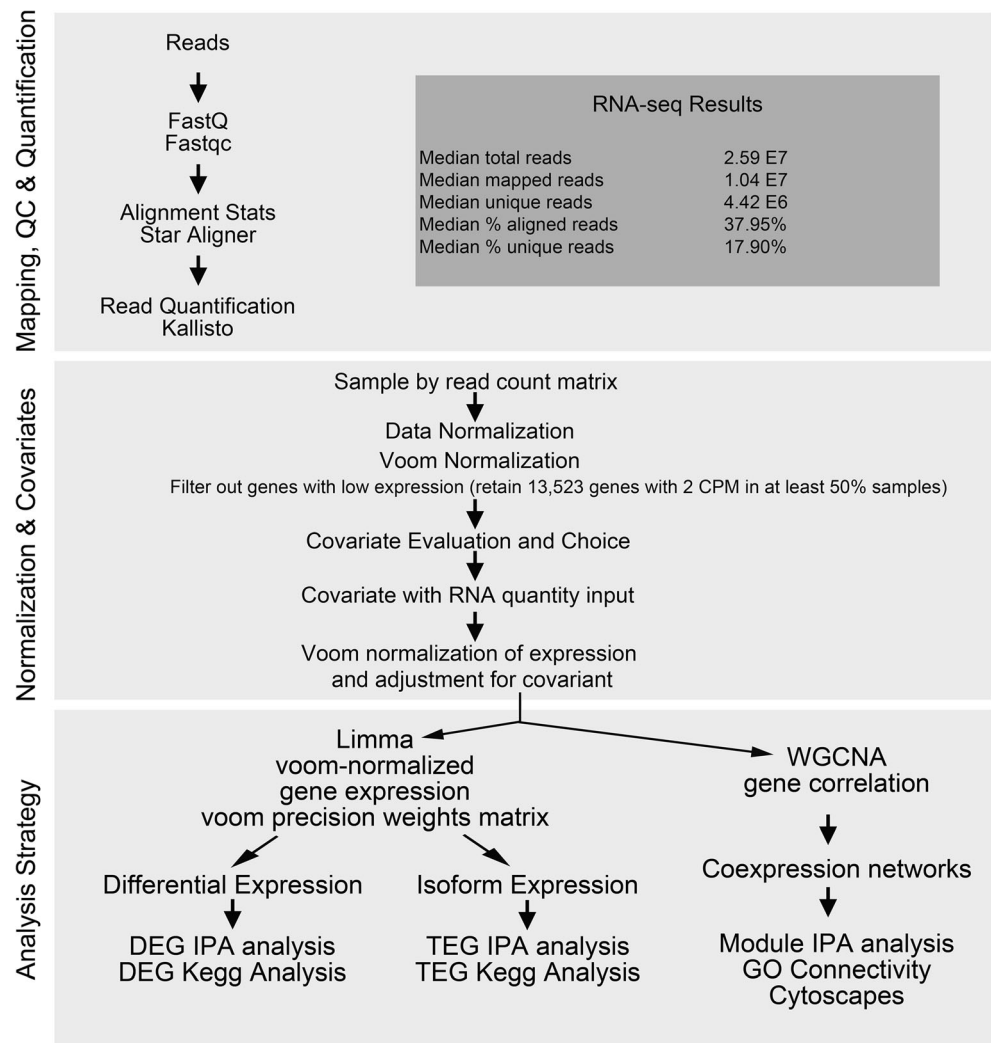
### MSN BFCN Single Population RNA-seq

RNA-seq was performed on BFCNs from Ts65Dn (Ts) and 2N mice (Fig. 1 and Supplemental Table 2). RNA-seq reads from BFCNs were mapped and normalization and covariate analyses were performed (Fig. 2 and Supplemental Fig. 1). Principal component analysis (PCA) revealed minimal variability in 2N BFCNs while greater variability was observed in Ts BFCNs (Fig. 3A). This likely reflects the onset of BFCN degeneration and indicates BFCN degeneration may have an epigenetic component. Differential expression analysis revealed 1443 of 13,523 genes were differentially expressed at  $p < 0.05$ , with 22 genes at FDR  $< 0.05$ . Analysis revealed 84.54% of DEGs were protein coding. The remaining DEGs were ncRNAs, pseudogenes, and microRNAs (miRNAs) (Fig. 3B). Heatmaps and volcano plots show individual genes differentially regulated in Ts BFCNs by LFC in individual samples and mean LFC and  $p$ -value (Fig. 3C, D). DEGs exhibited both upregulated (777) and downregulated (666) gene expression level changes in Ts BFCNs with LFCs ranging from 0.32 to 10.25 (Fig. 3E and Supplemental Table 3). Select DEGs are represented by violin plots across genotypes (Fig. 3F).

### DEGs Linked to DS

We queried DS murine orthologs triplicated in the Ts mouse model [67, 85], and 64 protein coding trisomic genes were expressed in MSN BFCNs. Ten genes were differentially expressed, with 8 upregulated and 2 downregulated (Fig. 4).

**Fig. 2** Pipeline for bioinformatic workflow using RNA-seq libraries derived from LCM-captured MSN BFCNs



Due to the low number of expression differences, we hypothesize BFCN degeneration likely involves additional factors than simply triplicated gene expression. Accordingly, DEGs were analyzed utilizing pathway analysis.

### IPA and KEGG analysis reveal novel pathways providing a molecular basis for vulnerability of trisomic BFCNs

Molecular pathways were examined that individual DEGs belong to by IPA and KEGG analysis (Figs. 5, 6). IPA analysis revealed 114 of the 161 significant pathways ( $-\log(p)$  value  $\geq 1.3$ ) were neuronal-relevant and dysregulated in Ts BFCNs (Table 1). We curated 20 pathways for in-depth analysis at the start of cholinergic degeneration (Fig. 5A). Several critical pathways were upregulated in trisomic BFCNs, including glutamate receptor signaling (Fig. 5B), synaptic long-term potentiation (Fig. 5C), CREB signaling in neurons (Fig. 5D), and calcium signaling (not shown). Downregulated pathways were also identified, including superpathway of cholesterol

biosynthesis (not shown), oxidative phosphorylation (Fig. 5E), and integrin signaling (not shown). Not surprisingly, several pathways showed redundancy in specific gene expression, including the glutamate receptor signaling, CREB signaling in neurons and long-term potentiation pathway genes.

KEGG analysis enabled a second independent bioinformatics approach. KEGG analysis identified 41 neuronal pathways (Table 2). We curated critical key pathways (Fig. 6A) including dysregulation in the cholinergic synapse (Fig. 6B). Interestingly, phospholipase C beta 2 (*Plcb2*) and protein kinase C gamma (*Prkcg*) were both upregulated and are positively linked to calcium signaling (identified as dysregulated by IPA; Table 1), while muscarinic receptor 2 (*Chrm2*) and G protein subunit beta5 (*Gnb5*) were downregulated and are involved in cell survival (Fig. 6B). The Alzheimer's disease pathway was novel to KEGG analysis (Fig. 6C) and identified several key DEGs disrupted within trisomic BFCNs. The GABA receptor signaling pathway (Fig. 6D) was identified by both IPA and KEGG analysis. KEGG also identified the neurotrophin signaling pathway (Fig. 6E) as significantly

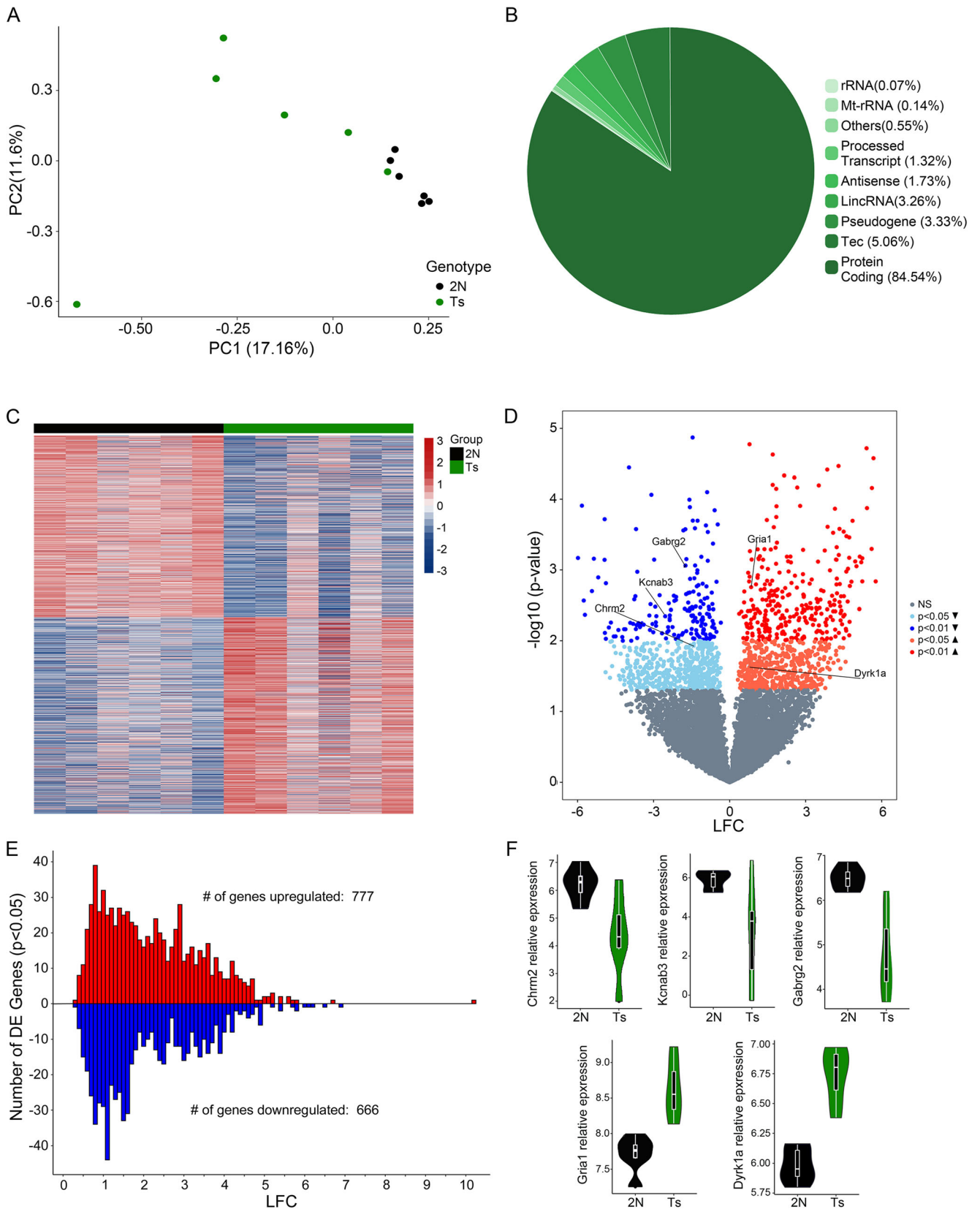


**Fig. 3** MSN BFCNs show significant differences in gene expression in 6 MO Ts and 2N mice. Study groups included trisomic (Ts,  $n = 6$ ) and normal disomic littermates (2N,  $n = 6$ ). **A** PCA plot shows clear differences between the 2N and Ts MSN BFCNs, with Ts mice displaying a broader range of gene expression variability. **B** Pie chart indicates 84.54% of gene expression differences in ChAT-immunopositive BFCNs are protein coding. **C** Heatmap illustrates DEGs in individual Ts and 2N mice. **D** Volcano plots show relative upregulation, downregulation, and LFC of Ts MSN BFCN gene expression differences on a  $-\log[10]$  of  $p$  value scale. Differential gene expression changes are expressed as log-fold change (LFC; red = Ts > 2N, blue = Ts < 2N). **E** Distribution of LFC of differential expression for 1443 DEGs. Ts MSN LFC for upregulated genes are plotted in red ( $n = 777$ , positive values), and Ts LFC for downregulated genes in blue ( $n = 666$ , negative values). **F** Violin plots show relative gene expression for select DEGs, with 2N in black and Ts in green

dysregulated. IPA and KEGG revealed overlapping and differing differentially regulated genes within many of these pathways (Tables 1 and 2).

### Transcript Analysis

To interrogate genes with multiple transcripts expressed in MSN neurons, we examined transcript expression (TEG) changes and compared them to DEGs. Comparing DEGs and TEGs ( $p < 0.05$ ), over half of identified transcripts were also significantly affected at the gene level (Supplemental Fig. 2A). IPA analysis revealed 17 of the top 20 pathways identified by DEG IPA were also significant by TEG IPA (Supplemental Fig. 2B). DEG and TEG overlap was found for the majority of genes within discrete pathways (Supplemental Fig. 2C-F), with some pathways showing notable differences. In TEGs, pathway analysis revealed  $-\log(p\text{-values})$  increased for many selected pathways, but the  $z$ -score

indicating directionality of pathway changes tended to decrease (Supplemental Table 4). This effectively resulted in transcript analysis detracting from effect sizes, which is likely due to identified TEGs with low expressing isoforms in neurons. Therefore, we pursued validation using different methodological approaches.

### Weighted Gene Co-expression Network Analysis (WGCNA)

We utilized a WGCNA approach to analyze the association of module expression (based on module eigengene) within BFCNs. The 13,523 genes expressed in the BFCN network were subdivided into 19 modules ranging from 78 to 2988 genes. Analysis revealed 2 modules with differential gene expression by genotype (FDR < 0.05; Fig. 7A). The Blue module contains 2124 genes, with ~68% of the genes upregulated in Ts BFCNs (Fig. 7B). The Black module contains 701 genes with ~66% of these upregulated in Ts BFCNs (Fig. 7B). STRING network analysis in Cytoscape was performed to determine physical interactions of encoded proteins within each module. Of the 2124 genes in the Blue module, STRING analysis identified 1721 proteins with 2999 interactions (Supplemental Fig. 3A), with insets highlighting close interactions in detail (Supplemental Fig. 3B-E). To query the most relevant genes, the top 500 significant gene hits in the Blue module were analyzed by STRING, with 428 identified proteins and 614 connections (Fig. 7C). Top interactions were discs large MAGUK scaffold protein 4 (*Dlg4*; also known as PSD-95), glutamate receptor, ionotropic, AMPA1 (*Gria1*), syntaxin 1A (*Stx1a*), adenylate cyclase 1 (*Adcy1*), and mitogen-activated protein kinase 3 (*Mapk3*). All 701 genes in the Black module were queried by STRING analysis, of

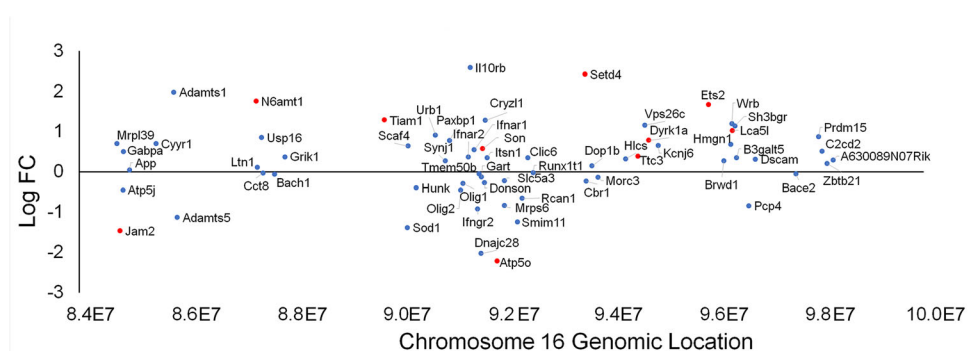


**Fig. 4** Trisomic protein coding genes do not necessarily match copy number within vulnerable cell types. In MSN BFCNs, only 64 genes (of 88) show quantifiable expression levels (in blue) (2 CPM in 50% of samples) with 10 genes attaining statistical significance at 6 MO (in red), including 8 upregulated {N-6 adenine-specific DNA methyltransferase1 (*N6amt1*), T cell lymphoma invasion and metastasis 1 (*Tiam1*), Son DNA binding protein (*Son*), SET domain containing 4 (*Setd4*), tetratricopeptide

repeat domain 3 (*Ttc3*), dual specificity tyrosine phosphorylation regulated kinase 1A (*Dyrk1a*), E26 avian leukemia oncogene 2,3' domain (*Ets2*) and lebercilin congenital amaurosis 5-like (*Lca5l*)} and 2 downregulated genes {junction adhesion molecule 2 (*Jam2*) and ATP synthase H+ transporting mitochondrial F1 complex, O subunit (*Atp5o*)}. Significant DEGs are depicted in red, and not differentially expressed genes depicted in blue

**Table 1** Significant IPA canonical pathways identified by DEG at ( $p < 0.05$ )

Ingenuity canonical pathways	$-\log(p \text{ value})$	Ratio	z-score
Oxidative phosphorylation	11.9	0.257	-5.292
Mitochondrial dysfunction	11.6	0.205	
Synaptogenesis signaling pathway	8.26	0.138	0.152
Sirtuin signaling pathway	7.22	0.134	2.414
Protein kinase A signaling	6.06	0.113	0.845
Calcium signaling	5.49	0.136	1.789
Glycolysis I	4.45	0.308	-2.828
GABA receptor signaling	3.41	0.147	
Superpathway of cholesterol biosynthesis	3.24	0.241	-2.646
Synaptic long-term potentiation	2.96	0.124	1.291
CREB signaling in neurons	2.92	0.106	1.698
IGF-1 signaling	2.54	0.125	-0.333
Type II diabetes mellitus signaling	2.53	0.113	-0.707
Cholesterol biosynthesis I	2.45	0.308	-2
PI3K/AKT signaling	2.34	0.103	-1.807
Synaptic long-term depression	2.33	0.101	2.524
Glutamate receptor signaling	2.05	0.14	1.342
Integrin signaling	1.8	0.0892	-2.183
Death receptor signaling	1.71	0.11	-1.265
Type I diabetes mellitus signaling	1.53	0.0991	-0.632
Axonal guidance signaling	3.61	0.0909	
ERK/MAPK signaling	1.92	0.0933	1
mTOR signaling	3.6	0.114	0
Sucrose degradation V (mammalian)	3.13	0.444	-1
GP6 signaling pathway	2.89	0.126	1.807
Inhibition of ARE-mediated mRNA degradation pathway	2.77	0.123	-0.775
NGF signaling	2.2	0.114	0.277
Clathrin-mediated endocytosis signaling	1.62	0.0881	
HIPPO signaling	1.49	0.106	1.89
TCA cycle II (eukaryotic)	5.76	0.375	-3
Estrogen receptor signaling	5.46	0.116	0.169
Gluconeogenesis I	5.42	0.346	-3
Huntington's disease signaling	5.2	0.127	0
Amyotrophic lateral sclerosis signaling	4.42	0.165	0.832
Tight junction signaling	4.2	0.131	
IL-8 signaling	3.92	0.12	-1.706
ILK signaling	3.84	0.121	-1.279
Opioid signaling pathway	3.65	0.109	1.569
Pyridoxal 5'-phosphate salvage pathway	3.32	0.169	-0.302
Gαq signaling	3.24	0.12	-0.243
Germ cell-Sertoli cell junction signaling	3.22	0.117	
nNOS SIGNALING IN NEURONS	3.21	0.191	0.816
GNRH signaling	3.16	0.116	0.775
cAMP-mediated signaling	3.07	0.105	0.218
Dopamine-DARPP32 feedback in cAMP signaling	3.07	0.117	1.698
14-3-3-mediated signaling	3.04	0.126	-0.632
Endocannabinoid neuronal synapse pathway	3	0.125	0.258
Melatonin signaling	2.93	0.153	0.302
BAG2 signaling pathway	2.83	0.186	-0.707

**Table 1** (continued)

Ingenuity canonical pathways	$-\log(p \text{ value})$	Ratio	z-score
Ceramide signaling	2.71	0.136	-1.265
Neuropathic pain signaling in dorsal horn neurons	2.66	0.129	1.387
Xenobiotic metabolism signaling	2.65	0.0941	
Chemokine signaling	2.55	0.138	-0.302
Thrombin signaling	2.54	0.101	0.5
Reelin signaling in neurons	2.54	0.116	-1.604
Gap junction signaling	2.45	0.101	
Cholesterol biosynthesis II (via 24,25-dihydrostanosterol)	2.45	0.308	-2
Cholesterol biosynthesis III (via desmosterol)	2.45	0.308	-2
Sertoli cell-Sertoli cell junction signaling	2.44	0.103	
Phospholipase C signaling	2.38	0.0934	0
Salvage pathways of pyrimidine ribonucleotides	2.35	0.124	-0.577
PPAR $\alpha$ /RXR $\alpha$ activation	2.31	0.1	0.5
Actin cytoskeleton signaling	2.31	0.0963	-0.447
Factors promoting cardiogenesis in vertebrates	2.29	0.107	3
Netrin signaling	2.2	0.138	1
CXCR4 signaling	2.2	0.102	-1
Mitotic roles of polo-like kinase	2.16	0.136	
p70S6K signaling	2.14	0.109	0.302
Regulation of eIF4 and p70S6K signaling	2.11	0.102	-0.816
Sphingosine-1-phosphate signaling	2.11	0.111	-0.277
G protein coupled receptor signaling	2.08	0.0882	
Protein ubiquitination pathway	2.06	0.0879	
Signaling by Rho family GTPases	2.06	0.0902	-1.789
eNOS signaling	2.06	0.101	0.577
Cholecystokinin/gastrin-mediated signaling	2.05	0.109	0.577
Regulation of actin-based motility by Rho	2.02	0.117	-0.905
Telomerase signaling	2.01	0.112	-1
Xenobiotic metabolism CAR signaling pathway	2.01	0.0952	-1.886
LPS-stimulated MAPK signaling	2	0.122	-0.632
$\alpha$ -Adrenergic signaling	1.95	0.115	1.134
Growth hormone signaling	1.95	0.127	1
Androgen signaling	1.94	0.103	0.632
Semaphorin signaling in neurons	1.92	0.133	
Ephrin B signaling	1.92	0.125	-0.378
Valine degradation I	1.91	0.222	-2
UVA-induced MAPK signaling	1.89	0.112	0.447
RhoGDI signaling	1.89	0.0944	1.291
Ephrin receptor signaling	1.89	0.0944	-0.302
Aryl hydrocarbon receptor signaling	1.77	0.0979	0
Mechanisms of viral exit from host cells	1.73	0.146	
Role of PKR in interferon induction and antiviral response	1.73	0.103	-0.302
Corticotropin releasing hormone signaling	1.72	0.0966	0.277
Xenobiotic metabolism PXR signaling pathway	1.64	0.0885	-1.213
IL-15 production	1.63	0.0992	0.577
Tec kinase signaling	1.62	0.0915	-0.577
EIF2 signaling	1.6	0.0848	-1.414
Phagosome maturation	1.59	0.0927	
Role of NFAT in regulation of the immune response	1.57	0.0884	0

**Table 1** (continued)

Ingenuity canonical pathways	$-\log(p \text{ value})$	Ratio	z-score
Neuregulin signaling	1.56	0.104	0
Role of CHK proteins in cell cycle checkpoint control	1.56	0.123	0
Adrenomedullin signaling pathway	1.55	0.0863	0.728
TR/RXR activation	1.52	0.107	
Senescence pathway	1.52	0.08	-0.426
PTEN signaling	1.5	0.0952	0.577
B cell receptor signaling	1.49	0.0865	-0.5
Apoptosis signaling	1.48	0.101	0.707
Apelin endothelial signaling pathway	1.43	0.0957	-0.302
Cell cycle regulation by BTG family proteins	1.38	0.135	
Wnt/Ca + pathway	1.38	0.113	1.89
Assembly of RNA polymerase II complex	1.35	0.12	
Docosahexaenoic acid (DHA) signaling	1.34	0.132	
Hepatic fibrosis signaling pathway	1.34	0.0734	0
UVC-induced MAPK signaling	1.32	0.118	0.816
IL-7 signaling pathway	1.31	0.103	-1.342

which 586 proteins with 1043 connections were observed (Fig. 7D). The top interactions in the Black module were block of proliferation 1 ribosomal biogenesis factor (*Bop1*), proliferation-associated 2G4 (*Pa2g4*), bystin like (*Bysl*), DEAD-box helicase 5 (*Ddx5*), and eukaryotic translation initiation factor 5B (*Eif5b*).

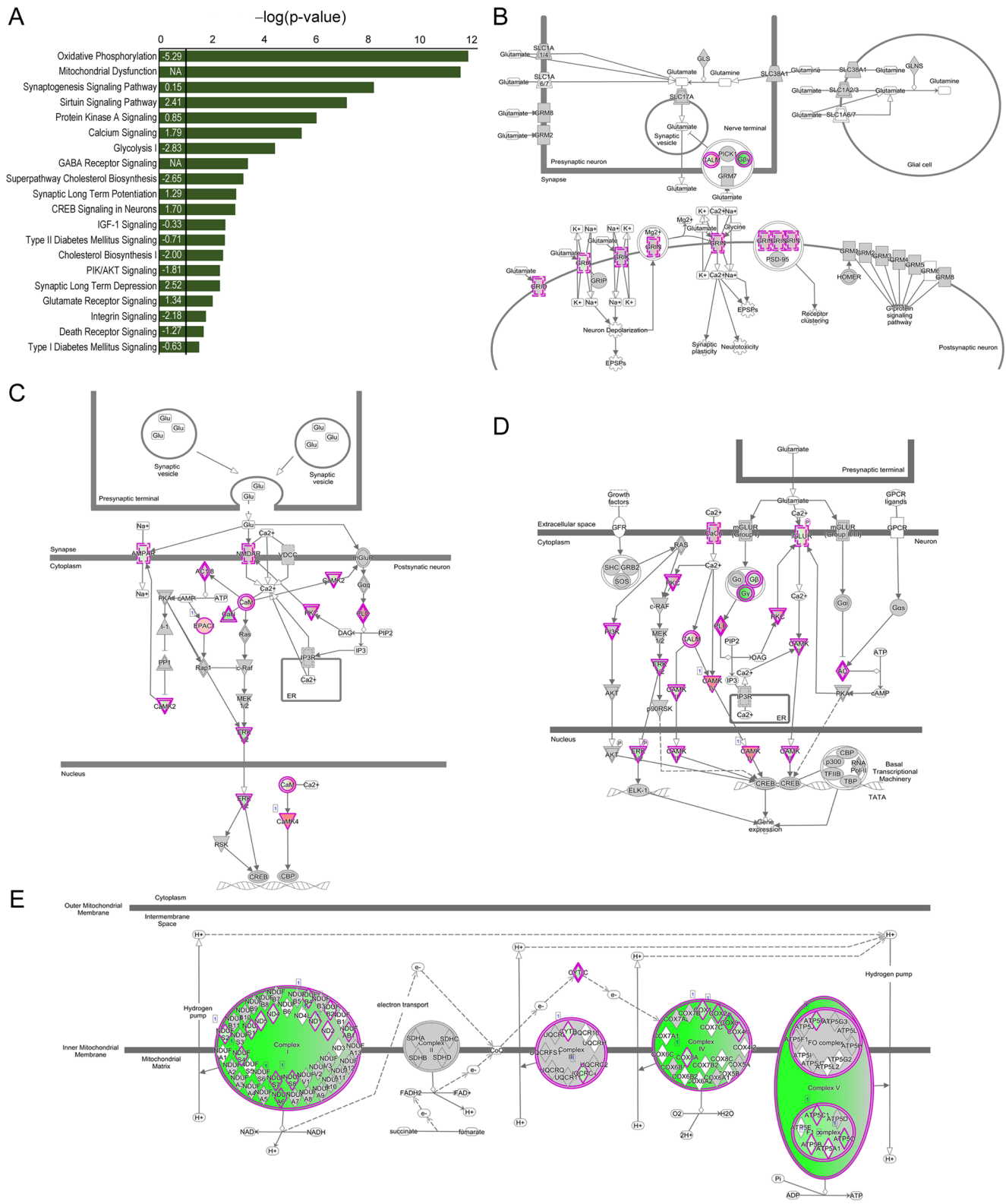
To compare the two methodologies (DEG and WGCNA) for functional pathway analysis, we performed IPA analysis on WGCNA Blue and Black modules. A total of 109 significantly affected neuronal pathways were found in the Blue module, of which 58 overlapped with DEG significant pathways (Fig. 8A). A total of 29 of 40 significantly affected pathways in the Black module replicated the DEG analysis (Fig. 8B). Therefore, the majority of significant pathways by DEG analysis are also significant by WGCNA analysis, confirming these methodologies. Importantly, 12 of the top 15 interesting pathways in the Blue module were also in the top 20 of the DEG IPA analysis (Fig. 8C, Supplemental Table 5), while in the Black module 4 of the top 10 were also in the top 20 of the DEG IPA analysis (Fig. 8D, Supplemental Table 6). Collectively, module data also revealed several significant pathways, including G beta gamma signaling and Neurotrophin/Trk Signaling for the Blue module (Fig. 8E, Supplemental Table 5) and focal adhesion kinase (FAK), Notch, and p53 signaling in the Black module (Fig. 8F, Supplemental Table 6).

### qRT-PCR Validation

qRT-PCR results showed positive correlations with several dysregulated genes by RNA-seq ( $R = 0.67$ ,  $p = 0.024$ ; Fig.

9A). *Chrm2* and *Mapk8* were significantly downregulated by RNA-seq and correlated with qRT-PCR results while *Prkcg*, *Grin2a*, and *Camk2a* were significantly upregulated by RNA-seq and correlated with qRT-PCR results (Fig. 9A, B). In addition, phospholipase C beta 1 (*Pccb1*), nerve growth factor receptor (*Ngfr/p75<sup>NTR</sup>*), and *Chrm1* were within dysregulated pathways identified by IPA or KEGG analysis, and while not significantly dysregulated by RNA-seq, they correlated with RNA-seq and qRT-PCR (Fig. 9A). In contrast, kinase D interacting substrate 220 (*Kidins220/Arms*) and neprilysin (*Mme*) were not differentially regulated by RNA-seq and did not correlate with qRT-PCR findings (Fig. 9A). *Mapk3* was the only gene queried by qRT-PCR which did not correlate to significant changes in RNA-seq findings (Fig. 9A, B), likely due to a combination gene change selectivity within BFCNs and low expression levels of this gene.

**Fig. 5** Bioinformatic assessment of vulnerable pathways in trisomic BFCNs by IPA. **A** IPA identified significant effects on 161 pathways, with select pathways depicted ( $-\log(p \text{ value})$ : significance of pathway dysregulation; z-scores (white in bars): upregulation (+) or downregulation (-), not accessible (NA). **B, C, D, E** Targeted pathways display significant dysregulation based on the highlighted gene expression changes (LFC, magenta outlines represent significant alterations, with pink fill indicating  $Ts > 2N$  and green fill indicating  $Ts < 2N$ ). **B** The glutamatergic pathway shows increased activation in trisomic BFCNs, which is also observed in **(C)** synaptic long-term potentiation and **D** the CREB signaling pathway. While the oxidative phosphorylation **E** pathway shows decreased activation in trisomic BFCNs



**Discussion**

We generated an expression profile of vulnerable MSN BFCNs in 6 MO trisomic mice without the confounding

transcriptomic signal of glia or other neuronal populations. Previous studies identified BFCN degeneration in Ts65Dn mice at 6 MO or older [21, 29, 31, 43, 86]. Therefore, our results suggest transcriptomic changes seen herein precede or

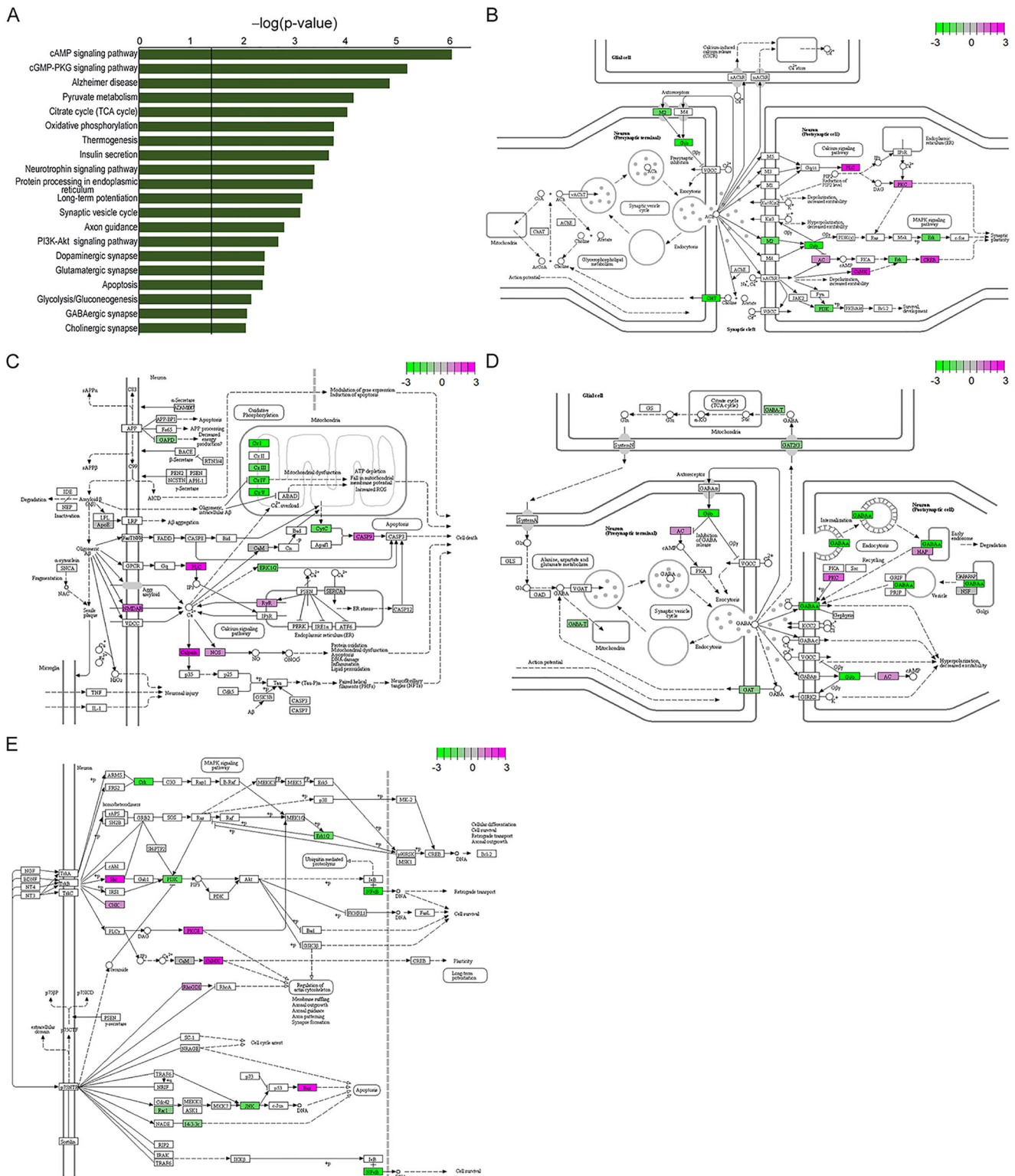


**Fig. 6** Bioinformatic assessment of vulnerable pathways in trisomic BFCNs by KEGG. **A** KEGG analysis revealed novel dysregulated pathways as well as several that overlapped with IPA analysis. **B** The cholinergic synapse is dysregulated with the *Chr2* receptor downregulated, leading to changes in synaptic plasticity. **C** The

Alzheimer’s disease pathway is dysregulated. **D** GABAergic and glutamatergic pathways (see Fig. 5B, for IPA analysis) both showed differential expression in trisomic BFCNs (LFC; pink Ts > 2N, green Ts < 2N). **E** Neurotrophin signaling pathway deficits implicate a decrease

**Table 2** Significant KEGG analysis pathways identified by DEG at ( $p < 0.05$ )

ID	Description	GeneRatio	BgRatio	<i>p</i> value	<i>p</i> value adj	<i>q</i> -value	Count
mmu04024	cAMP signaling pathway	33/539	215/8756	8.82123E-07	8.70362E-05	6.407E-05	33
mmu04022	cGMP-PKG signaling pathway	27/539	173/8756	6.38541E-06	0.000210009	0.000154594	27
mmu05010	Alzheimer disease	41/539	333/8756	1.42254E-05	0.000382791	0.000281785	41
mmu00620	Pyruvate metabolism	10/539	38/8756	7.07092E-05	0.001395328	0.001027144	10
mmu00020	Citrate cycle (TCA cycle)	9/539	32/8756	9.27335E-05	0.00171557	0.001262884	9
mmu00190	Oxidative phosphorylation	20/539	133/8756	0.000169671	0.002811728	0.0020698	20
mmu04714	Thermogenesis	29/539	230/8756	0.000170983	0.002811728	0.0020698	29
mmu04911	Insulin secretion	15/539	86/8756	0.000211094	0.003124191	0.002299813	15
mmu04722	Neurotrophin signaling pathway	18/539	121/8756	0.000406091	0.005008461	0.003686883	18
mmu04141	Protein processing in endoplasmic reticulum	22/539	164/8756	0.000434643	0.005146174	0.003788257	22
mmu04720	Long-term potentiation	12/539	67/8756	0.000696835	0.006910116	0.00508675	12
mmu04721	Synaptic vesicle cycle	13/539	77/8756	0.000759582	0.00725278	0.005338995	13
mmu04360	Axon guidance	22/539	180/8756	0.001534914	0.013767711	0.010134837	22
mmu04151	PI3K-Akt signaling pathway	36/539	355/8756	0.002021361	0.017050027	0.012551051	36
mmu04728	Dopaminergic synapse	17/539	135/8756	0.003715829	0.026677091	0.01963783	17
mmu04724	Glutamatergic synapse	15/539	113/8756	0.003785263	0.026677091	0.01963783	15
mmu04210	Apoptosis	17/539	136/8756	0.004011903	0.027616823	0.020329596	17
mmu00010	Glycolysis/gluconeogenesis	10/539	66/8756	0.006691175	0.039611756	0.029159437	10
mmu04727	GABAergic synapse	12/539	89/8756	0.008068003	0.045925554	0.033807218	12
mmu04725	Cholinergic synapse	14/539	112/8756	0.008603028	0.047394141	0.03488829	14
mmu04925	Aldosterone synthesis and secretion	20/539	100/8756	2.23743E-06	0.00011038	8.1254E-05	20
mmu04960	Aldosterone-regulated sodium reabsorption	9/539	38/8756	0.000386834	0.00497839	0.003664746	9
mmu05014	Amyotrophic lateral sclerosis (ALS)	11/539	58/8756	0.00070035	0.006910116	0.00508675	11
mmu01230	Biosynthesis of amino acids	12/539	77/8756	0.002438012	0.018503882	0.013621279	12
mmu01200	Carbon metabolism	23/539	120/8756	8.61286E-07	8.70362E-05	6.407E-05	23
mmu04961	Endocrine and other factor-regulated calcium reabsorption	13/539	60/8756	5.59168E-05	0.001182241	0.000870284	13
mmu04666	Fc gamma R-mediated phagocytosis	12/539	90/8756	0.008806344	0.047394141	0.03488829	12
mmu04510	Focal adhesion	26/539	199/8756	0.000207789	0.003124191	0.002299813	26
mmu04066	HIF-1 signaling pathway	16/539	112/8756	0.001307045	0.012090171	0.008899948	16
mmu05016	Huntington disease	40/539	268/8756	1.29621E-07	3.8368E-05	2.82438E-05	40
mmu04211	Longevity regulating pathway	12/539	90/8756	0.008806344	0.047394141	0.03488829	12
mmu04978	Mineral absorption	11/539	52/8756	0.000259915	0.003497039	0.002574278	11
mmu04932	Non-alcoholic fatty liver disease (NAFLD)	18/539	150/8756	0.004834532	0.03180048	0.023409315	18
mmu04921	Oxytocin signaling pathway	18/539	153/8756	0.005948338	0.037916892	0.027911794	18
mmu05012	Parkinson disease	22/539	142/8756	5.12707E-05	0.001167394	0.000859355	22
mmu00640	Propanoate metabolism	8/539	33/8756	0.000689043	0.006910116	0.00508675	8
mmu04974	Protein digestion and absorption	15/539	94/8756	0.00057103	0.006260186	0.004608316	15
mmu04964	Proximal tubule bicarbonate reclamation	9/539	22/8756	2.86599E-06	0.00012119	8.92119E-05	9
mmu04723	Retrograde endocannabinoid signaling	24/539	148/8756	1.07353E-05	0.000317765	0.000233916	24
mmu04530	Tight junction	19/539	166/8756	0.006438165	0.038891774	0.028629435	19

pace subsequent neuronal degeneration, a key finding. Not surprisingly, the profile of trisomic BFCN degeneration is more complex than simply the triplication of the “DS critical region,” for which we provide pathway analysis from numerous genes expressed on non-triplicated chromosomes. Importantly, the present DEG and WGCNA bioinformatics

platforms analyzed by IPA and KEGG highlight the critical need for multiple bioinformatics approaches to reveal the mechanistic potential of analyzing single population RNA-seq datasets within vulnerable cell types.

Dysregulated genes in the oxidative phosphorylation pathway are also implicated in AD pathology [87]. These genes

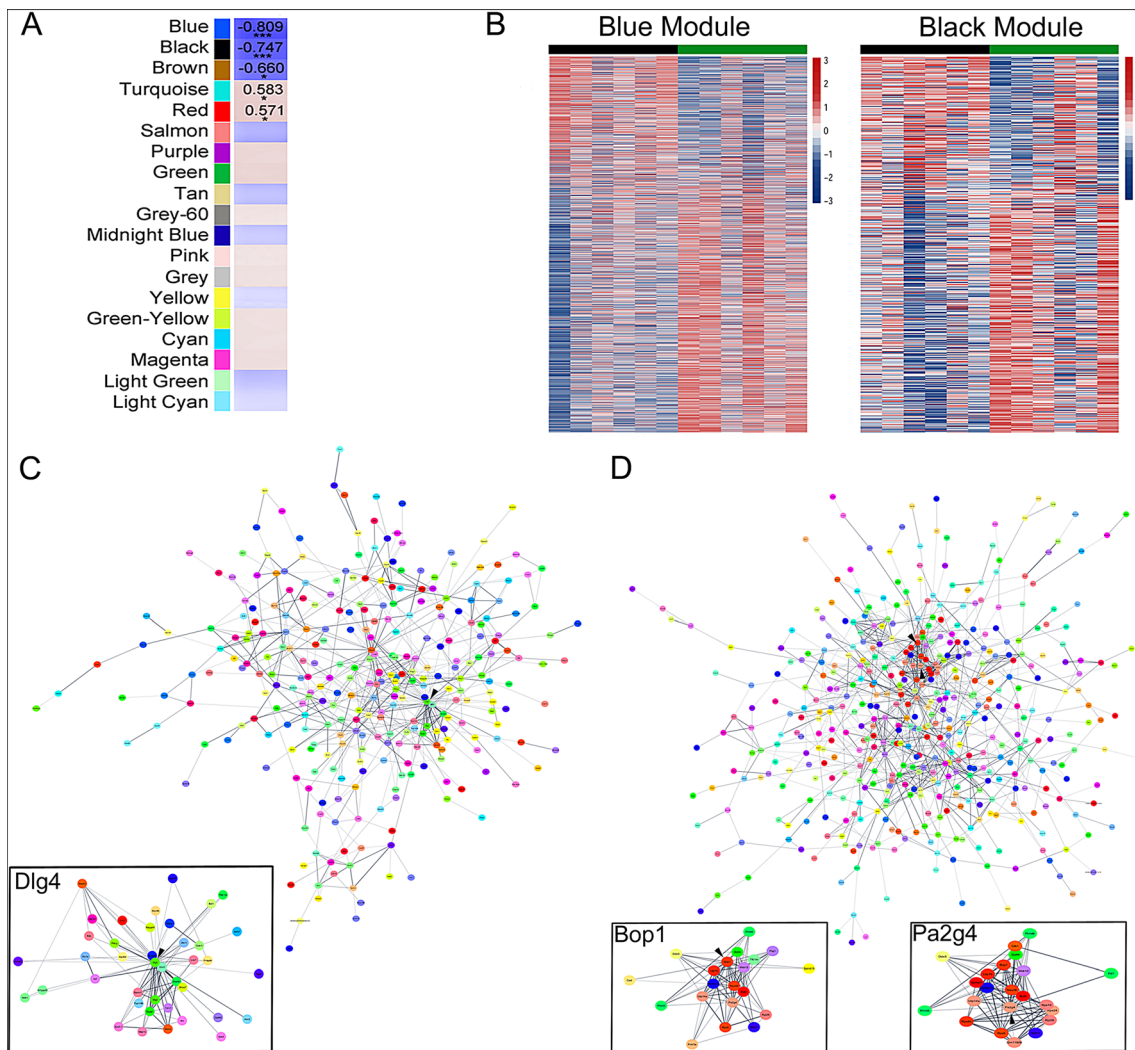


**Fig. 7** Whole-genome co-expression network analysis in MSN BFCNs. **A** Control-derived modules ranked by enrichment status. The Blue module ( $-0.809$ ) and Black module ( $-0.747$ ) revealed significant gene expression differences by genotype within MSN BFCNs at FDR ( $<0.05$ ). **B** Heatmaps indicating the Blue module contains 2199 genes and the Black module contains 701 genes. **C** The top 500 genes in the Blue module

were queried by STRING in Cytoscape to examine protein interactions. Dlg4 (PSD-95) showed 41 direct protein-protein interactions within the top 500 (inset). **D** All 701 genes in the Black module were queried by STRING in Cytoscape. Bop1 and Pa2g4 had the highest number [17] of direct interactions (insets). \* ( $p < 0.05$ ), \*\*\*\* FDR ( $<0.05$ )

include mitochondrially encoded NADH dehydrogenases (*Mt-Nd1*, *Mt-Nd2*, *Mt-Nd 4*, and *Mt-Nd5*), along with NADH:ubiquinone oxidoreductase subunits (*Ndufa6*, *Ndufab1*, *Ndufb2*, *Ndufb4*, *Ndufs1*, *Ndufs2*, *Ndufs4*, *Ndufs7*, and *Ndufs8*) (Fig. 5E). Results indicate energy metabolism is strongly disrupted, identifying a direct mechanistic link previously postulated between oxidative stress [29] and neurodegeneration in DS/AD, and may serve as novel therapeutic target candidates to deter BFCN degeneration.

Trisomic MSN BFCNs display upregulation of select glutamate receptor transcripts (Fig. 5B), similar to findings within the hippocampus [19, 47, 48, 88–90], contributing to disruption of long-term potentiation (LTP) and long-term depression (LTD) in Ts65Dn mice [91–94]. We also observed downregulation of genes involved in GABAergic neurotransmission.

Paradoxically, the majority of hippocampal studies in Ts65Dn mice report upregulation of several GABA<sub>A</sub> receptor subunits and increased inhibition of LTP [89, 91, 92, 95–97]. Discrepancies in gene expression point to the key differences between our single population approach in BFCNs relative to mixed hippocampal population analyses.

CREB signaling, along with many downstream effectors, is also dysregulated in trisomic BFCNs (Fig. 5D). While previous associations have linked CREB expression with downregulation of key genes in DS, including somatostatin and cell division protein control 42 [98], we observed generalized increased CREB pathway expression by IPA analysis. We found increased CREB signaling and upregulation of several calcium channel and glutamate receptor subunits as well as downstream calcium calmodulin dependent kinases and

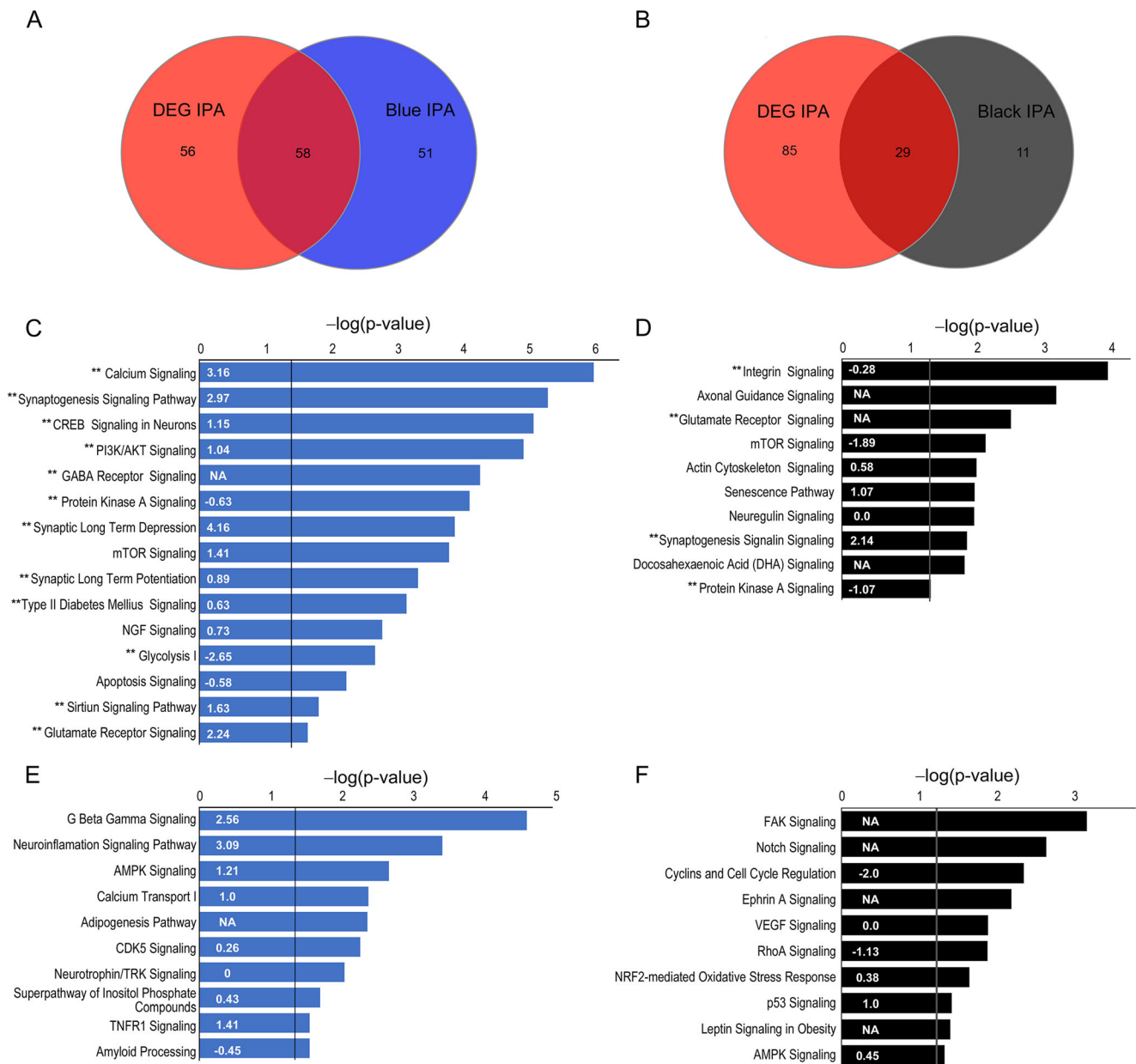


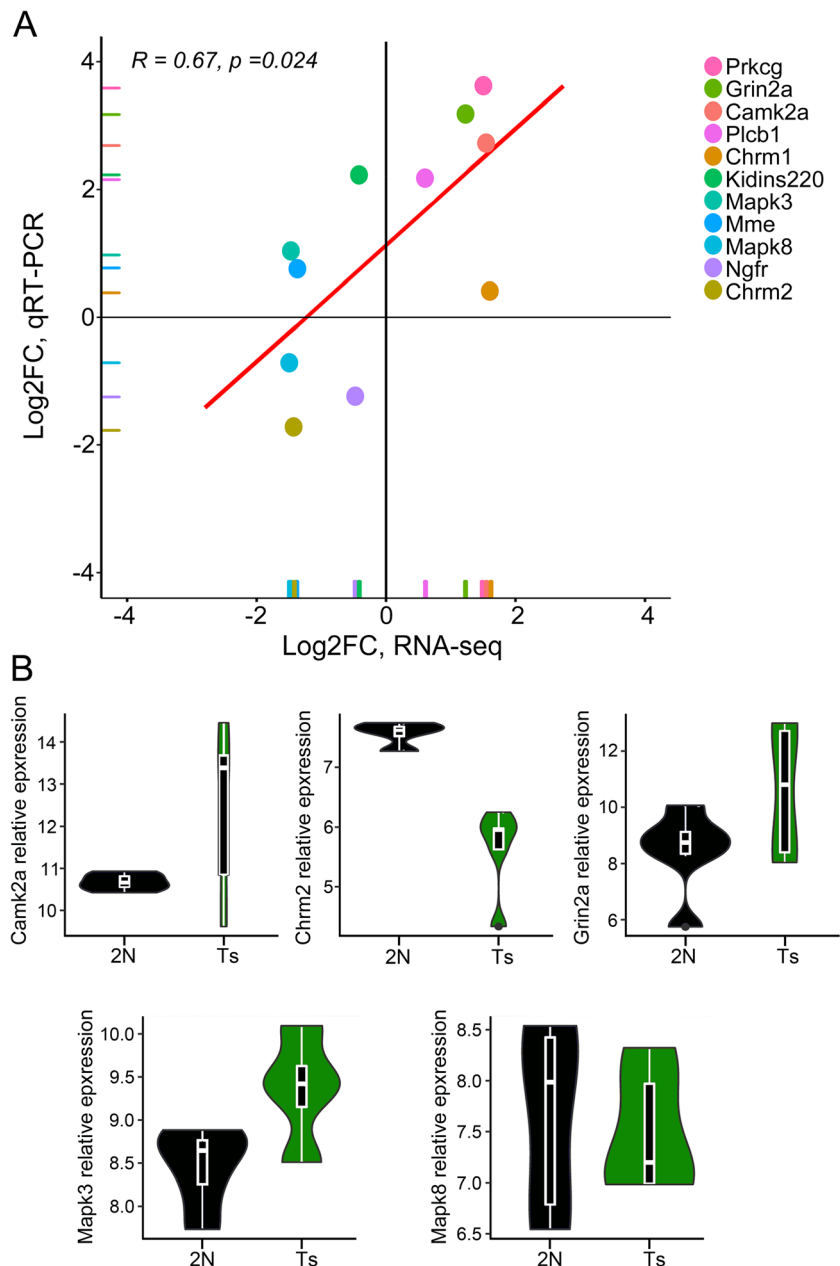
**Fig. 8** WGCNA Blue and Black modules were queried for pathway changes by IPA. **A** Venn diagram shows overlap of genes and pathways identified by both DEG ( $p < 0.05$ ) and the Blue module. **B** Venn diagram shows majority of dysregulated pathways in Black module overlap with DEG pathways. **C** Pathways significant to both the Blue module and DEG are shown with  $-\log(p\text{ value})$  and  $z$ -scores

phospholipase C isoforms, which has been previously seen in aging in the Ts65Dn model [44] [48, 99]. Furthermore, alterations in neurotrophin receptor signaling does not include discrete neurotrophin receptors or *Bdnf*. Rather, significant alterations in the neurotrophin pathway include several downstream key regulators of apoptosis, LTP, and cell survival. Interestingly, TrkA (*Ntrk1*) gene expression is not significantly different between genotypes ~6 MO but is a key gene in the Blue module with a median 1.7-fold decrease in expression in

in white text. **D** A few pathways significant to both Black module and DEG were identified (double asterisks (\*\*)) indicating pathways highlighted by DEG analysis). Pathways in the **E** Blue module and **F** Black module that were not significantly affected by DEG at  $p < 0.05$  are depicted

trisomic MSN BFCNs, which may indicate TrkA is affected by BFCN degeneration, as dysregulation is observed in older Ts65Dn mice [21]. Downregulation of TrkA expression has also been observed within human postmortem BFCNs during AD progression and correlates with cognitive decline and Braak stage [17, 100–107]. Furthermore, we demonstrate downregulation of several downstream effector genes of the NGF-TrkA pathway crucial for BFCN survival including phosphatidylinositol 3-kinase catalytic subunit (*Pik3ca*), v-

**Fig. 9** **A** qRT-PCR results for 11 genes {calcium/calmodulin dependent protein kinase II alpha (*Camk2a*), cholinergic receptor muscarinic 1 (*Chrm1*), *Chrm2*, glutamate ionotropic receptor NDMA type subunit 2A (*Grin2a*), *Kidins220/Arms*, *Mapk3* (aka *Erk1*), mitogen-activated protein kinase 8 (*Mapk8* aka *Erk2*), *Mme*, *Ngfr/p75<sup>NTR</sup>*, *Plcb1*, and *Prkcg*} interrogated from Nissl-stained MSN neurons correlate strongly with RNA-seq data obtained from ChAT-positive MSN BFCNs ( $R = 0.67$ ,  $p = 0.024$ ). **B** Violin plots show relative gene expression values for a subset of the interrogated genes. *Camk2a*, *Chrm2*, *Grin2a*, *Mapk3*, and *Mapk8* are all significantly dysregulated by RNA-seq in Ts MSN BFCNs. Of these, only *Mapk3* qRT-PCR does not replicate the directionality of the LFC seen in the RNA-seq data. (black = 2N; green = Ts)



rel reticuloendotheliosis viral oncogene homolog A (*Rela*), and calmodulin 3 (*Calm3*) in trisomic BFCNs, indicating the relevance of this pathway in this established AD and DS model.

We identified vulnerabilities by KEGG within the cholinergic synapse, further indicating this target for therapeutic intervention. Notably, *Chrm2*, encoding the muscarinic M2 cholinergic receptor and primarily localized to ChAT-positive cholinergic neurons [108, 109], was downregulated along with downstream effectors *Gnb5*, which leads to downregulation of *Mapk3*, causing dampening of synaptic plasticity [110]. In addition, presynaptic choline transferase is downregulated, along with *Chrm2* and *Gnb5* which block choline

uptake and calcium to the presynaptic terminal [111]. Conversely, *Plcb2* and *Prkcg*, downstream of the muscarinic M1 cholinergic receptor, are upregulated, likely driving the increases seen in the calcium signaling pathway [112, 113]. These novel findings in vulnerable BFCNs have translational implications, as muscarinic cholinergic receptors have relatively limited expression throughout the forebrain, and represent realistic candidates to slow or stop the BFCN degeneration that is seen in both DS and AD.

KEGG analysis also revealed significant dysregulation of genes involved in AD pathogenesis including apolipoprotein E (*ApoE*), calpain 1 (*Capn1*), nitric oxide synthase 1 (*Nos1*) and glyceraldehyde-3-phosphate dehydrogenase (*Gapdh*) [68,

69]. Interestingly, there is a small but significant decrease in ApoE expression in Ts BFCNs. The ApoE e4 isoform is known to drive AD pathology [70]. Low plasma levels of ApoE ApoE were observed in subjects with severe dementia, correlating with cognitive decline [71]. Increases in Capn1 activation have previously been linked to AD pathology [114, 115]. Increased active Capn1 results in increased cerebrospinal fluid levels of neurogranin in AD patients [116], while inhibition results in improved cholinergic function in rats [117]. Capn1 activation is also linked to type II diabetes mellitus, and pathways linked to diabetes and metabolic syndrome are dysregulated in Ts BFCNs [114]. *Nos1*, upregulated in Ts BFCNs, also shows increased expression in AD [118, 119] and GWAS studies implicate aberrant *Nos1* expression in AD [120]. Reduction in *Gapdh* activity has also been shown in AD brain due to oxidative modification [121]. A component of AD dysfunction involves deficits in mitochondrial activity and oxidative phosphorylation, paralleling the present findings. In Ts BFCNs, the ATP synthase H<sup>+</sup>-transporting mitochondrial F1 complex, alpha subunit 1 (*Atp5a1*), cytochrome c oxidase subunit 4I1 (*Cox4i1*), and *Ndufs4* were dysregulated (Fig. 6C), as well as numerous genes within the oxidative phosphorylation pathway (Fig. 5E). Moreover, several Alzheimer's disease pathway dysregulated genes within Ts BFCNs replicate key findings in a human AD study examining miRNA and RNA expression profiling from the GEO database [122], indicating trisomic BFCN degeneration is likely caused by early AD-relevant gene expression changes.

Combined WGCNA and STRING analysis indicate *Dlg4* (PSD-95) has direct interactions with numerous significantly dysregulated genes and pathways, including glutamate receptor signaling, synaptogenesis signaling, and neurotrophin signaling. These results suggest that *Dlg4* may be a hub in the degenerative pathways of BFCNs. Changes in *Dlg4* have been linked to early synapse loss in AD mouse models and human postmortem AD studies [122, 123]. WGCNA analysis also shows significant pathway dysregulation in amyloid processing, calcium transport, FAK, and Notch signaling in trisomic BFCNs. Importantly, these individual genes and key pathways would not have been identified without individual cell population RNA-seq, as the relatively low abundance and very specific expression patterns would have likely been masked in admixed cell type or regional RNA-seq analysis.

Bioinformatic pathway analysis of trisomic BFCNs shows significant changes in many relevant pathways including excitatory and inhibitory neurotransmission, resulting in LTP and LTD changes, synaptic plasticity, along with changes in oxidative states and mitochondrial dysfunction. These results point towards mechanisms underlying BFCN degeneration which have direct translational implications for both DS and AD pathobiology and therapeutic intervention. Limitations of the current work include variability in RNA quality. Genotype

differences in RNA quality is unlikely, as previous qRT-PCR studies from subregional dissections have not revealed genotype effects [45, 47–49], and RNA quantity was normalized as a covariate during analysis. This initial study was performed in male mice, and sex differences may exist in BFCN degenerative programs [22]. A second cohort of trisomic female mice is currently in progress, although previous work from mixed sex studies have not revealed significant differences in select gene expression [45, 48, 49]. Several mouse models recapitulate aspects of the human trisomic phenotype. These models have varying numbers of triplicated HSA21 orthologs, including Dp16/Dp17/Dp10 (168), Tc1 (124), Dp16 (106), Ts65Dn/Ts2 (94), and Ts1Cje (74) [85, 124–126]. The Ts65Dn model is the most widely used and is notable for septohippocampal degeneration and behavioral deficits that mimic DS and AD endophenotypes [124, 127–129]. However, the Ts65Dn mouse model does not recapitulate the full pathobiology of DS or AD. Future assessments will consider evaluating BFCN degeneration from other models in relation to postmortem changes in BFCNs from DS and AD brains.

## Conclusions

We provide single population expression profiling of BFCNs at a key timepoint, at the initiation of neurodegenerative programs, to understand mechanisms driving AD pathogenesis utilizing a trisomic model. We uncovered select genes in key signaling pathways that likely underlie BFCN degeneration, which will help the field rationally design therapeutic strategies aimed at preserving the septohippocampal circuit without targeting ancillary neuronal and non-neuronal populations.

**Abbreviations** *Adcy1*, adenylate cyclase 1; AD, Alzheimer's disease; *ApoE*, apolipoprotein E; *Atp5a1*, ATP synthase H<sup>+</sup>-transporting mitochondrial F1 complex, alpha subunit 1; *Atp5o*, ATP synthase H<sup>+</sup>-transporting mitochondrial F1 complex, O subunit; BFCN, basal forebrain cholinergic neuron; *Bop1*, block of proliferation 1 ribosomal biogenesis factor; *Bdnf*, brain derived neurotrophin factor; *Bystl*, bystin like; *Camk2a*, calcium/calmodulin dependent protein kinase II alpha; *Calm3*, calmodulin 3; *Capn1*, calpain 1; ChAT, choline acetyltransferase; CPM, counts per million; *Cox4i1*, cytochrome c oxidase subunit 4I1; *Ddx5*, DEAD-box helicase 5; DEG, differentially expressed gene; *Dlg4*, also known as PSD-95, discs large MAGUK scaffold protein 4; 2N, disomic; DS, Down syndrome; *Dyrk1a*, dual specificity tyrosine phosphorylation regulated kinase 1A; *Ets2*, E26 avian leukemia oncogene 2,3' domain; *Eif5b*, eukaryotic translation initiation factor 5B; FDR, false discovery rate; FAK, focal adhesion kinase; *Gnb5*, G protein subunit beta5; *Gusb*, glucuronidase beta; *Grin2a*, glutamate ionotropic receptor NDMA type subunit 2A; *Gria1*, glutamate receptor, ionotropic, AMPA1; *Gapdh*, glyceraldehyde-3-phosphate dehydrogenase; HSA21, human chromosome 21; IPA, Ingenuity Pathway Analysis; *Jam2*, junction adhesion molecule 2; *Kidins220/Arms*, kinase D interacting substrate 220; KEGG, Kyoto Encyclopedia of Genes and Genomes; LCM, laser capture microdissection; *Lca5l*, lebercilin congenital amaurosis 5-like; LFC, log-

fold change; LTD, long-term depression; LTP, long-term potentiation; MSN, medial septal nucleus; miRNAs, microRNAs; *Mapk8 aka Erk2*, mitogen-activated protein kinase 8; *Mapk3*, mitogen-activated protein kinase 3; MO, months of age; *Chrm1*, muscarinic cholinergic receptor 1; *Chrm2*, muscarinic cholinergic receptor 2; *N6amt1*, N-6 adenine-specific DNA methyltransferase1; *Mt-Nd1*, *Mt-Nd2*, *Mt-Nd 4*, and *Mt-Nd5*, NADH dehydrogenases; *Ndufa6*, *Ndufab1*, *Ndufb2*, *Ndufb4*, *Ndufs1*, *Ndufs2*, *Ndufs4*, *Ndufs7*, and *Ndufs8*, NADH:ubiquinone oxidoreductase subunits; *Mme*, neprilysin; *Ngfr/p75NTR*, nerve growth factor receptor; *Nos1*, nitric oxide synthase 1; ncRNA, noncoding RNA; *Pik3ca*, phosphatidylinositol 3-kinase catalytic subunit; *Plcb1*, phospholipase C beta 1; *Plcb2*, phospholipase C beta 2; PEN, polyethylene naphthalate; PCA, principal component analysis; *Pa2g4*, proliferation-associated 2G4; *Prkcg*, protein kinase C gamma; QC, quality control; RNA-seq, RNA sequencing; RT, room temperature; *Setd4*, SET domain containing 4; *Son*, Son DNA binding protein; *Stx1a*, syntaxin 1A; *Tiam1*, T cell lymphoma invasion and metastasis 1; *Tic3*, tetratricopeptide repeat domain 3; TEG, transcript expression; *Ntrk1*, TrkA; Ts, Ts65Dn; Rela, v-rel reticuloendotheliosis viral oncogene homolog A; WGCNA, weighted gene co-expression network analysis

**Supplementary Information** The online version contains supplementary material available at <https://doi.org/10.1007/s12035-021-02453-3>.

**Acknowledgments** We thank Arthur Saltzman, M.S. and Paul Zappile, M.S. for expert technical assistance.

**Authors' Contributions** MJA, SCP, AH, PR, and SDG designed the experiments. MJA and SCP performed the experiments. MJA, SCP, PR, and SDG performed the statistical analysis. MJA and SDG wrote manuscript. All authors read and approved final manuscript.

**Funding** Funding was provided by support from grants AG014449, AG043375, AG055328, and AG017617 from the National Institutes of Health and the Alzheimer's Association.

**Data Availability** Data analyzed within this study are included in this body of the manuscript and within the supplementary information files. Data are also available from the corresponding author upon request.

## Declarations

**Ethics approval** Animal protocols were approved by the Nathan Kline Institute/NYU Grossman School of Medicine Animal Care and Use Committee (IACUC) in accordance with NIH guidelines.

**Competing interests** The authors declare that they have no competing interests.

## References

- Parker SE, Mai CT, Canfield MA, Rickard R, Wang Y, Meyer RE, Anderson P, Mason CA et al (2010) Updated National Birth prevalence estimates for selected birth defects in the United States, 2004–2006. *Birth Defects Res A Clin Mol Teratol* 88:1008–1016
- Presson AP, Partyka G, Jensen KM, Devine OJ, Rasmussen SA, McCabe LL et al (2013) Current estimate of Down Syndrome population prevalence in the United States. *J Pediatr* 163(4):1163–1168
- Mann DM, Yates PO, Marcyniuk B (1984) Alzheimer's presenile dementia, senile dementia of Alzheimer type and Down's syndrome in middle age form an age related continuum of pathological changes. *Neuropathol Appl Neurobiol* 10:185–207
- Coyle JT, Oster-Granite ML, Reeves RH, Gearhart JD (1988) Down syndrome, Alzheimer's disease and the trisomy16 mouse. *Trends Neurosci* 11(9):390–394
- Hook EB (1989) Issues pertaining to the impact and etiology of trisomy 21 and other aneuploidy in humans; a consideration of evolutionary implications, maternal age mechanisms, and other matters. *Prog Clin Biol Res* 311:1–27
- Hodgkins PS, Prasher V, Farrar G, Armstrong R, Sturman S, Corbett J, Blair JA (1993) Reduced transferrin binding in Down syndrome: a route to senile plaque formation and dementia. *Neuroreport* 5(1):21–24
- Roth GM, Sun B, Greensite FS, Lott IT, Dietrich RB (1996) Premature aging in persons with Down syndrome: MR findings. *AJNR Am J Neuroradiol* 17(7):1283–1289
- Chapman RS, Hesketh LJ (2000) Behavioral phenotype of individuals with Down syndrome. *Ment Retard Dev Disabil Res Rev* 6:84–95
- Cataldo AM, Peterhoff CM, Troncoso JC, Gomez-Isla T, Hyman BT, Nixon RA (2000) Endocytic pathway abnormalities precede amyloid beta deposition in sporadic Alzheimer's disease and Down syndrome: differential effects of APOE genotype and presenilin mutations. *Am J Pathol* 157:277–286
- Hartley D, Blumenthal T, Carrillo M, DiPaolo G, Esralew L, Gardiner K, Granholm AC, Iqbal K et al (2015) Down syndrome and Alzheimer's disease: common pathways, common goals. *Alzheimers Dement* 11:700–709
- Hartley SL, Handen BL, Devenny DA, Hardison R, Mihaila I, Price JC, Cohen AD, Klunk WE et al (2014) Cognitive functioning in relation to brain amyloid-beta in healthy adults with Down syndrome. *Brain* 137:2556–2563
- Leverenz JB, Raskind MA (1998) Early amyloid deposition in the medial temporal lobe of young Down syndrome patients: a regional quantitative analysis. *Exp Neurol* 150:296–304
- Wisniewski KE, Dalton AJ, Crapper McLachlan DR, Wen GY, Wisniewski HM (1985) Alzheimer's disease in Down's syndrome: clinicopathologic studies. *Neurology* 35:957–961
- Lai F, Williams RS (1989) A prospective study of Alzheimer disease in Down syndrome. *Arch Neurol* 46(8):849–853
- Perez SE, Miguel JC, He B, Malek-Ahmadi M, Abrahamson EE, Ikonovic MD, Lott I, Doran E et al (2019) Frontal cortex and striatal cellular and molecular pathobiology in individuals with Down syndrome with and without dementia. *Acta Neuropathol* 137(3):413–436
- Sendera TJ, Ma SY, Jaffar S, Kozlowski PB, Kordower JH, Mawal Y, Saragovi HU, Mufson EJ (2000) Reduction in TrkA-immunoreactive neurons is not associated with an overexpression of galaninergic fibers within the nucleus basalis in Down's syndrome. *J Neurochem* 74(3):1185–1196
- Mufson EJ, Bothwell M, Kordower JH (1989) Loss of nerve growth factor receptor-containing neurons in Alzheimer's disease: a quantitative analysis across subregions of the basal forebrain. *Exp Neurol* 105:221–232
- Mann DM, Yates PO, Marcyniuk B, Ravindra CR (1986) The topography of plaques and tangles in Down's syndrome patients of different ages. *Neuropathol Appl Neurobiol* 12:447–457
- Belichenko PV, Kleschevnikov AM, Masliah E, Wu C, Takimoto-Kimura R, Salehi A, Mobley WC (2009) Excitatory-inhibitory relationship in the fascia dentata in the Ts65Dn mouse model of Down syndrome. *J Comp Neurol* 512:453–466
- Belichenko PV, Masliah E, Kleschevnikov AM, Villar AJ, Epstein CJ, Salehi A, Mobley WC (2004) Synaptic structural abnormalities in the Ts65Dn mouse model of Down Syndrome. *J Comp Neurol* 480:281–298

21. Granholm AC, Sanders LA, Crnic LS (2000) Loss of cholinergic phenotype in basal forebrain coincides with cognitive decline in a mouse model of Down's syndrome. *Exp Neurol* 161:647–663
22. Kelley CM, Powers BE, Velazquez R, Ash JA, Ginsberg SD, Strupp BJ, Mufson EJ (2014) Sex differences in the cholinergic basal forebrain in the Ts65Dn mouse model of Down syndrome and Alzheimer's disease. *Brain Pathol* 24:33–44
23. Kelley CM, Powers BE, Velazquez R, Ash JA, Ginsberg SD, Strupp BJ, Mufson EJ (2014) Maternal choline supplementation differentially alters the basal forebrain cholinergic system of young-adult Ts65Dn and disomic mice. *J Comp Neurol* 522:1390–1410
24. Betts MJ, Kirilina E, Otaduy MCG, Ivanov D, Acosta-Cabrero J, Callaghan MF, Lambert C, Cardenas-Blanco A et al (2019) Locus coeruleus imaging as a biomarker for noradrenergic dysfunction in neurodegenerative diseases. *Brain*. 142(9):2558–2571
25. Yamasaki M, Takeuchi T (2017) Locus coeruleus and dopamine-dependent memory consolidation. *Neural Plast* 2017:8602690
26. Teixeira CM, Rosen ZB, Suri D, Sun Q, Hersh M, Sargin D et al (2018) Hippocampal 5-HT input regulates memory formation and Schaffer collateral excitation. *Neuron* 98(5):992–1004.e4
27. Sekeres MJ, Winocur G, Moscovitch M (2018) The hippocampus and related neocortical structures in memory transformation. *Neurosci Lett* 680:39–53
28. Solari N, Hangya B (2018) Cholinergic modulation of spatial learning, memory and navigation. *Eur J Neurosci* 48(5):2199–2230
29. Lockrow J, Prakasam A, Huang P, Bimonte-Nelson H, Sambamurti K, Granholm AC (2009) Cholinergic degeneration and memory loss delayed by vitamin E in a Down syndrome mouse model. *Exp Neurol* 216(2):278–289
30. Hunter CL, Bimonte-Nelson HA, Nelson M, Eckman CB, Granholm AC (2004) Behavioral and neurobiological markers of Alzheimer's disease in Ts65Dn mice: effects of estrogen. *Neurobiol Aging* 25(7):873–884
31. Holtzman DM, Santucci D, Kilbridge J, Chua-Couzens J, Fontana DJ, Daniels SE, Johnson RM, Chen K et al (1996) Developmental abnormalities and age-related neurodegeneration in a mouse model of Down syndrome. *Proc Natl Acad Sci U S A* 93:13333–13338
32. Cooper JD, Salehi A, Delcroix JD, Howe CL, Belichenko PV, Chua-Couzens J, Kilbridge JF, Carlson EJ et al (2001) Failed retrograde transport of NGF in a mouse model of Down's syndrome: reversal of cholinergic neurodegenerative phenotypes following NGF infusion. *Proc Natl Acad Sci U S A* 98(18):10439–10444
33. Powers BE, Kelley CM, Velazquez R, Ash JA, Strawderman MS, Alldred MJ, Ginsberg SD, Mufson EJ et al (2017) Maternal choline supplementation in a mouse model of Down syndrome: effects on attention and nucleus basalis/substantia innominata neuron morphology in adult offspring. *Neuroscience*. 340:501–514
34. Powers BE, Velazquez R, Kelley CM, Ash JA, Strawderman MS, Alldred MJ, Ginsberg SD, Mufson EJ et al (2016) Attentional function and basal forebrain cholinergic neuron morphology during aging in the Ts65Dn mouse model of Down syndrome. *Brain Struct Funct* 221:4337–4352
35. Ash JA, Velazquez R, Kelley CM, Powers BE, Ginsberg SD, Mufson EJ, Strupp BJ (2014) Maternal choline supplementation improves spatial mapping and increases basal forebrain cholinergic neuron number and size in aged Ts65Dn mice. *Neurobiol Dis* 70:32–42
36. Kelley CM, Ash JA, Powers BE, Velazquez R, Alldred MJ, Ikonomic MD, Ginsberg SD, Strupp BJ et al (2016) Effects of maternal choline supplementation on the septohippocampal cholinergic system in the Ts65Dn mouse model of Down syndrome. *Curr Alzheimer Res* 13:84–96
37. Strupp BJ, Powers BE, Velazquez R, Ash JA, Kelley CM, Alldred MJ, Strawderman M, Caudill MA et al (2016) Maternal choline supplementation: a potential prenatal treatment for Down syndrome and Alzheimer's disease. *Curr Alzheimer Res* 13:97–106
38. Moon J, Chen M, Gandhi SU, Strawderman M, Levitsky DA, Maclean KN, Strupp BJ (2010) Perinatal choline supplementation improves cognitive functioning and emotion regulation in the Ts65Dn mouse model of Down syndrome. *Behav Neurosci* 124:346–361
39. Hunter CL, Bimonte HA, Granholm A-CE (2003) Behavioral comparison of 4 and 6 month-old Ts65Dn mice: age-related impairments in working and reference memory. *Behav Brain Res* 138(2):121–131
40. Kelley CM, Ginsberg SD, Alldred MJ, Strupp BJ, Mufson EJ (2019) Maternal choline supplementation alters basal forebrain cholinergic neuron gene expression in the Ts65Dn Mouse model of down syndrome. *Dev Neurobiol* 79(7):664–683
41. Cataldo AM, Petanceska S, Peterhoff CM, Terio NB, Epstein CJ, Villar A, Carlson EJ, Staufenbiel M et al (2003) App gene dosage modulates endosomal abnormalities of Alzheimer's disease in a segmental trisomy 16 mouse model of Down syndrome. *J Neurosci* 23:6788–6792
42. Hunter CL, Isacson O, Nelson M, Bimonte-Nelson H, Seo H, Lin L, Ford K, Kindy MS et al (2003) Regional alterations in amyloid precursor protein and nerve growth factor across age in a mouse model of Down's syndrome. *Neurosci Res* 45(4):437–445
43. Contestabile A, Fila T, Bartesaghi R, Ciani E (2006) Choline acetyltransferase activity at different ages in brain of Ts65Dn mice, an animal model for Down's syndrome and related neurodegenerative diseases. *J Neurochem* 97(2):515–526
44. Ahmed MM, Block A, Tong S, Davison MT, Gardiner KJ (2017) Age exacerbates abnormal protein expression in a mouse model of Down syndrome. *Neurobiol Aging* 57:120–132
45. Alldred MJ, Chao HM, Lee SH, Beilin J, Powers BE, Petkova E, Strupp BJ, Ginsberg SD (2018) CA1 pyramidal neuron gene expression mosaics in the Ts65Dn murine model of Down syndrome and Alzheimer's disease following maternal choline supplementation. *Hippocampus*. 28(4):251–268
46. Alldred MJ, Duff KE, Ginsberg SD (2012) Microarray analysis of CA1 pyramidal neurons in a mouse model of tauopathy reveals progressive synaptic dysfunction. *Neurobiol Dis* 45:751–762
47. Ginsberg SD (2010) Alterations in discrete glutamate receptor subunits in adult mouse dentate gyrus granule cells following perforant path transection. *Anal Bioanal Chem* 397:3349–3358
48. Alldred MJ, Lee SH, Petkova E, Ginsberg SD (2015) Expression profile analysis of hippocampal CA1 pyramidal neurons in aged Ts65Dn mice, a model of Down syndrome (DS) and Alzheimer's disease (AD). *Brain Struct Funct* 220:2983–2996
49. Alldred MJ, Chao HM, Lee SH, Beilin J, Powers BE, Petkova E, Strupp BJ, Ginsberg SD (2019) Long-term effects of maternal choline supplementation on CA1 pyramidal neuron gene expression in the Ts65Dn mouse model of Down syndrome and Alzheimer's disease. *FASEB J* 33(9):9871–9884
50. Eberwine J, Crino P, Dichter M (1995) Single-cell mRNA amplification: implications for basic and clinical neuroscience. *Neuroscientist* 1:200–211
51. Eberwine J, Kacharina JE, Andrews C, Miyashiro K, McIntosh T, Becker K, Barrett T, Hinkle D et al (2001) mRNA expression analysis of tissue sections and single cells. *J Neurosci* 21(21):8310–8314
52. Ginsberg SD, Crino PB, Hemby SE, Weingarten JA, Lee VM, Eberwine JH et al (1999) Predominance of neuronal mRNAs in individual Alzheimer's disease senile plaques. *Ann Neurol* 45:174–181
53. Ginsberg SD, Elarova I, Ruben M, Tan F, Counts SE, Eberwine JH, Trojanowski JQ, Hemby SE et al (2004) Single-cell gene

- expression analysis: implications for neurodegenerative and neuropsychiatric disorders. *Neurochem Res* 29:1053–1064
54. Baugh LR, Hill AA, Brown EL, Hunter CP (2001) Quantitative analysis of mRNA amplification by in vitro transcription. *Nucleic Acids Res* 29(5):e29–e229
  55. Colangelo V, Schurr J, Ball MJ, Pelaez RP, Bazan NG, Lukiw WJ (2002) Gene expression profiling of 12633 genes in Alzheimer hippocampal CA1: transcription and neurotrophic factor down-regulation and up-regulation of apoptotic and pro-inflammatory signaling. *J Neurosci Res* 70(3):462–473
  56. Dafforn A, Chen P, Deng G, Herrler M, Iglehart D, Koritala S, Lato S, Pillarisetty S et al (2004) Linear mRNA amplification from as little as 5 ng total RNA for global gene expression analysis. *BioTechniques*. 37(5):854–857
  57. Alldred MJ, Che S, Ginsberg SD (2009) Terminal continuation (TC) RNA amplification without second strand synthesis. *J Neurosci Methods* 177:381–385
  58. Alldred MJ, Che S, Ginsberg SD (2008) Terminal continuation (TC) RNA amplification enables expression profiling using minute RNA input obtained from mouse brain. *Int J Mol Sci* 9:2091–2104
  59. Zhang W, Yu Y, Hertwig F, Thierry-Mieg J, Zhang W, Thierry-Mieg D, Wang J, Furlanello C et al (2015) Comparison of RNA-seq and microarray-based models for clinical endpoint prediction. *Genome Biol* 16:133
  60. Mantione KJ, Kream RM, Kuzelova H, Ptacek R, Raboch J, Samuel JM, Stefano GB (2014) Comparing bioinformatic gene expression profiling methods: microarray and RNA-Seq. *Med Sci Monit Basic Res* 20:138–142
  61. Dong Z, Chen Y (2013) Transcriptomics: advances and approaches. *Sci China Life Sci* 56(10):960–967
  62. Wang Z, Gerstein M, Snyder M (2009) RNA-Seq: a revolutionary tool for transcriptomics. *Nat Rev Genet* 10(1):57–63
  63. Tang F, Barbacioru C, Wang Y, Nordman E, Lee C, Xu N, Wang X, Bodeau J et al (2009) mRNA-seq whole-transcriptome analysis of a single cell. *Nat Methods* 6(5):377–382
  64. Trombetta JJ, Gennert D, Lu D, Satija R, Shalek AK, Regev A (2014) Preparation of single-cell RNA-seq libraries for next generation sequencing. *Curr Protoc Mol Biol* 107:1–17
  65. Kim T, Lim CS, Kaang BK (2015) Cell type-specific gene expression profiling in brain tissue: comparison between TRAP. *LCM RNA-seq BMB Rep* 48:388–394
  66. Farris S, Wang Y, Ward JM, Dudek SM (2017) Optimized method for robust transcriptome profiling of minute tissues using laser capture microdissection and low-input RNA-seq. *Front Mol Neurosci* 10:185
  67. Duchon A, Raveau M, Chevalier C, Nalesso V, Sharp AJ, Herault Y (2011) Identification of the translocation breakpoints in the Ts65Dn and Ts1Cje mouse lines: relevance for modeling Down syndrome. *Mamm Genome* 22:674–684
  68. Wang X, Wang W, Li L, Perry G, Lee HG, Zhu X (2014) Oxidative stress and mitochondrial dysfunction in Alzheimer's disease. *Biochim Biophys Acta* 1842(8):1240–1247
  69. Swerdlow RH (2018) Mitochondria and mitochondrial cascades in Alzheimer's disease. *J Alzheimers Dis* 62(3):1403–1416
  70. Yamazaki Y, Zhao N, Caulfield TR, Liu CC, Bu G (2019) Apolipoprotein E and Alzheimer disease: pathobiology and targeting strategies. *Nat Rev Neurol* 15(9):501–518
  71. Predecki M, Florczak-Wyspianska J, Kowalska M, Ilkowski J, Grzelak T, Bialas K, Kozubski W, Dorszewska J (2019) APOE genetic variants and apoE, miR-107 and miR-650 levels in Alzheimer's disease. *Folia Neuropathol* 57(2):106–116
  72. Bray NL, Pimentel H, Melsted P, Pachter L (2016) Near-optimal probabilistic RNA-seq quantification. *Nat Biotechnol* 34(5):525–527
  73. Law CW, Chen Y, Shi W, Smyth GK (2014) Voom: precision weights unlock linear model analysis tools for RNA-seq read counts. *Genome Biol* 15(2):R29
  74. Ritchie ME, Phipson B, Wu D, Hu Y, Law CW, Shi W et al (2015) Limma powers differential expression analyses for RNA-sequencing and microarray studies. *Nucleic Acids Res* 43(7):e47
  75. Pages HCM, Falcon, S.; Li, N. AnnotationDbi: manipulation of SQLite-based annotations in bioconductor. 2019.
  76. Broberg P (2005) A comparative review of estimates of the proportion unchanged genes and the false discovery rate. *BMC Bioinform* 6:199
  77. Qiagen. <https://www.qiagenbioinformatics.com/products/ingenuity-pathway-analysis>. Accessed 29 Sept 2020
  78. Krämer A, Green J, Pollard J Jr, Tugendreich S (2013) Causal analysis approaches in ingenuity pathway analysis. *Bioinformatics (Oxford, England)* 30(4):523–530
  79. Kanehisa M, Goto S (2000) KEGG: kyoto encyclopedia of genes and genomes. *Nucleic Acids Res* 28(1):27–30
  80. Szklarczyk D, Gable AL, Lyon D, Junge A, Wyder S, Huerta-Cepas J et al (2018) STRING v11: protein–protein association networks with increased coverage, supporting functional discovery in genome-wide experimental datasets. *Nucleic Acids Res* 47(D1):D607–DD13
  81. Shannon P, Markiel A, Ozier O, Baliga NS, Wang JT, Ramage D, Amin N, Schwikowski B et al (2003) Cytoscape: a software environment for integrated models of biomolecular interaction networks. *Genome Res* 13(11):2498–2504
  82. Ginsberg SD, Alldred MJ, Counts SE, Cataldo AM, Neve RL, Jiang Y, Wu J, Chao MV et al (2010) Microarray analysis of hippocampal CA1 neurons implicates early endosomal dysfunction during Alzheimer's disease progression. *Biol Psychiatry* 68:885–893
  83. Jiang Y, Mullaney KA, Peterhoff CM, Che S, Schmidt SD, Boyer-Boiteau A, Ginsberg SD, Cataldo AM et al (2010) Alzheimer's-related endosome dysfunction in Down syndrome is Abeta-independent but requires APP and is reversed by BACE-1 inhibition. *Proc Natl Acad Sci U S A* 107:1630–1635
  84. ABI (2004) Guide to Performing relative quantitation of gene expression using real-time quantitative PCR. In: *Applied Biosystems Product Guide*, pp. 1–60
  85. Sturgeon X, Gardiner KJ (2011) Transcript catalogs of human chromosome 21 and orthologous chimpanzee and mouse regions. *Mamm Genome* 22:261–271
  86. Chen Y, Dyakin VV, Branch CA, Ardekani B, Yang D, Guilfoyle DN, Peterson J, Peterhoff C et al (2009) In vivo MRI identifies cholinergic circuitry deficits in a Down syndrome model. *Neurobiol Aging* 30:1453–1465
  87. Birnbaum JH, Wanner D, Gietl AF, Saake A, Kundig TM, Hock C, Nitsch RM, Tackenberg C (2018) Oxidative stress and altered mitochondrial protein expression in the absence of amyloid- $\beta$  and tau pathology in iPSC-derived neurons from sporadic Alzheimer's disease patients. *Stem Cell Res* 27:121–130
  88. Rueda N, Llorens-Martin M, Florez J, Valdizan E, Banerjee P, Trejo JL et al (2010) Memantine normalizes several phenotypic features in the Ts65Dn mouse model of Down syndrome. *J Alzheimers Dis* 21:277–290
  89. Souchet B, Guedj F, Penke-Verdier Z, Daubigney F, Duchon A, Herault Y et al (2015) Pharmacological correction of excitation/inhibition imbalance in Down syndrome mouse models. *Front Behav Neurosci* 9:267
  90. Kaur G, Sharma A, Xu W, Gerum S, Alldred MJ, Subbanna S, Basavarajappa BS, Pawlik M et al (2014) Glutamatergic transmission aberration: a major cause of behavioral deficits in a murine model of Down's syndrome. *J Neurosci* 34:5099–5106

91. Costa AC, Grybko MJ (2005) Deficits in hippocampal CA1 LTP induced by TBS but not HFS in the Ts65Dn mouse: a model of Down syndrome. *Neurosci Lett* 382(3):317–322
92. Kleschevnikov AM, Belichenko PV, Villar AJ, Epstein CJ, Malenka RC, Mobley WC (2004) Hippocampal long-term potentiation suppressed by increased inhibition in the Ts65Dn mouse, a genetic model of Down syndrome. *J Neurosci* 24(37):8153–8160
93. Siarey RJ, Carlson EJ, Epstein CJ, Balbo A, Rapoport SI, Galdzicki Z (1999) Increased synaptic depression in the Ts65Dn mouse, a model for mental retardation in Down syndrome. *Neuropharmacology*. 38(12):1917–1920
94. Siarey RJ, Stoll J, Rapoport SI, Galdzicki Z (1997) Altered long-term potentiation in the young and old Ts65Dn mouse, a model for Down syndrome. *Neuropharmacology*. 36(11-12):1549–1554
95. Block A, Ahmed MM, Rueda N, Hernandez MC, Martinez-Cue C, Gardiner KJ (2018) The GABA $\alpha$ 5-selective modulator, RO4938581, rescues protein anomalies in the Ts65Dn mouse model of Down syndrome. *Neuroscience*. 372:192–212
96. Colas D, Chuluun B, Warriar D, Blank M, Wetmore DZ, Buckmaster P, Garner CC, Heller HC (2013) Short-term treatment with the GABA $\alpha$  receptor antagonist pentylentetrazole produces a sustained pro-cognitive benefit in a mouse model of Down's syndrome. *Br J Pharmacol* 169:963–973
97. Kleschevnikov AM, Belichenko PV, Gall J, George L, Nosheny R, Maloney MT, Salehi A, Mobley WC (2012) Increased efficiency of the GABA $\alpha$  and GABA $\beta$  receptor-mediated neurotransmission in the Ts65Dn mouse model of Down syndrome. *Neurobiol Dis* 45(2):683–691
98. Sriroopreddy R, Sajeed R, Raghuraman, P, Sudandiradoss, C (2019) Differentially expressed gene (DEG) based protein-protein interaction (PPI) network identifies a spectrum of gene interactome, transcriptome and correlated miRNA in nondisjunction Down syndrome. *Int J Biol Macromol* 122:1080–1089
99. Alldred MJ, Lee SH, Petkova E, Ginsberg SD (2015) Expression profile analysis of vulnerable CA1 pyramidal neurons in young-Middle-Aged Ts65Dn mice. *J Comp Neurol* 523(1):61–74
100. Counts SE, Che S, Ginsberg SD, Mufson EJ (2011) Gender differences in neurotrophin and glutamate receptor expression in cholinergic nucleus basalis neurons during the progression of Alzheimer's disease. *J Chem Neuroanat* 42:111–117
101. Counts SE, Nadeem M, Wu J, Ginsberg SD, Saragovi HU, Mufson EJ (2004) Reduction of cortical TrkA but not p75(NTR) protein in early-stage Alzheimer's disease. *Ann Neurol* 56:520–531
102. Ginsberg SD, Che S, Wu J, Counts SE, Mufson EJ (2006) Down regulation of trk but not p75NTR gene expression in single cholinergic basal forebrain neurons mark the progression of Alzheimer's disease. *J Neurochem* 97:475–487
103. Latina V, Caioli S, Zona C, Ciotti MT, Amadoro G, Calissano P (2017) Impaired NGF/TrkA signaling causes early AD-linked presynaptic dysfunction in cholinergic primary neurons. *Front Cell Neurosci* 11:68
104. Mufson EJ, Li JM, Sobreviela T, Kordower JH (1996) Decreased trkA gene expression within basal forebrain neurons in Alzheimer's disease. *Neuroreport*. 8(1):25–29
105. Ginsberg SD, Mufson EJ, Alldred MJ, Counts SE, Wu J, Nixon RA, Che S (2011) Upregulation of select rab GTPases in cholinergic basal forebrain neurons in mild cognitive impairment and Alzheimer's disease. *J Chem Neuroanat* 42:102–110
106. Mufson EJ, Counts SE, Ginsberg SD (2002) Gene expression profiles of cholinergic nucleus basalis neurons in Alzheimer's disease. *Neurochem Res* 27:1035–1048
107. Mufson EJ, Counts SE, Ginsberg SD, Mahady L, Perez SE, Massa SM, Longo FM, Ikonovic MD (2019) Nerve growth factor pathobiology during the progression of Alzheimer's disease. *Front Neurosci* 13:533
108. Mufson EJ, Ginsberg SD, Ikonovic MD, DeKosky ST (2003) Human cholinergic basal forebrain: chemoanatomy and neurologic dysfunction. *J Chem Neuroanat* 26:233–242
109. Levey AI, Edmunds SM, Hersch SM, Wiley RG, Heilman CJ (1995) Light and electron microscopic study of m2 muscarinic acetylcholine receptor in the basal forebrain of the rat. *J Comp Neurol* 351(3):339–356
110. Fajardo-Serrano A, Liu L, Mott DD, McDonald AJ (2017) Evidence for M2 muscarinic receptor modulation of axon terminals and dendrites in the rodent basolateral amygdala: an ultrastructural and electrophysiological analysis. *Neuroscience*. 357: 349–362
111. Khaziev E, Samigullin D, Zhilyakov N, Fatikhov N, Bukharaeva E, Verkhatsky A et al (2016) Acetylcholine-induced inhibition of presynaptic calcium signals and transmitter release in the frog neuromuscular junction. *Front Physiol* 7:621
112. Lee J, Hwang YJ, Shin JY, Lee WC, Wie J, Kim KY, Lee MY, Hwang D et al (2013) Epigenetic regulation of cholinergic receptor M1 (CHRM1) by histone H3K9me3 impairs Ca(2+) signaling in Huntington's disease. *Acta Neuropathol* 125(5):727–739
113. Dippel E, Kalkbrenner F, Wittig B, Schultz G (1996) A heterotrimeric G protein complex couples the muscarinic m1 receptor to phospholipase C-beta. *Proc Natl Acad Sci U S A* 93(4): 1391–1396
114. Liu Y, Liu F, Grundke-Iqbal I, Iqbal K, Gong CX (2011) Deficient brain insulin signalling pathway in Alzheimer's disease and diabetes. *J Pathol* 225(1):54–62
115. Saito K, Elce JS, Hamos JE, Nixon RA (1993) Widespread activation of calcium-activated neutral proteinase (calpain) in the brain in Alzheimer disease: a potential molecular basis for neuronal degeneration. *Proc Natl Acad Sci U S A* 90(7):2628–2632
116. Becker B, Nazir FH, Brinkmalm G, Camporesi E, Kvartsberg H, Portelius E, Boström M, Kalm M et al (2018) Alzheimer-associated cerebrospinal fluid fragments of neurogranin are generated by Calpain-1 and prolyl endopeptidase. *Mol Neurodegener* 13(1):47
117. Kling A, Jantos K, Mack H, Hornberger W, Drescher K, Nimmrich V, Relo A, Wicke K et al (2017) Discovery of novel and highly selective inhibitors of calpain for the treatment of Alzheimer's disease: 2-(3-Phenyl-1H-pyrazol-1-yl)-nicotinamides. *J Med Chem* 60(16):7123–7138
118. Lüth HJ, Münch G, Arendt T (2002) Aberrant expression of NOS isoforms in Alzheimer's disease is structurally related to nitrotyrosine formation. *Brain Res* 953(1-2):135–143
119. Lüth HJ, Ogunlade V, Kuhla B, Kientsch-Engel R, Stahl P, Webster J, Arendt T, Münch G (2005) Age- and stage-dependent accumulation of advanced glycation end products in intracellular deposits in normal and Alzheimer's disease brains. *Cereb Cortex* 15(2):211–220
120. Lukiw WJ, Rogae EI (2017) Genetics of aggression in Alzheimer's disease (AD). *Front Aging Neurosci* 9:87
121. Butterfield DA, Hardas SS, Lange ML (2010) Oxidatively modified glyceraldehyde-3-phosphate dehydrogenase (GAPDH) and Alzheimer's disease: many pathways to neurodegeneration. *J Alzheimers Dis* 20(2):369–393
122. Chang WS, Wang YH, Zhu XT, Wu CJ (2017) Genome-wide profiling of miRNA and mRNA expression in Alzheimer's disease. *Med Sci Monit* 23:2721–2731
123. Hong S, Beja-Glasser VF, Nfonoyim BM, Frouin A, Li S, Ramakrishnan S et al (2016) Complement and microglia mediate early synapse loss in Alzheimer mouse models. *Science* 352(6286):712–716
124. Gupta M, Dhanasekaran AR, Gardiner KJ (2016) Mouse models of Down syndrome: gene content and consequences. *Mamm Genome* 27(11-12):538–555

125. Choong XY, Tosh JL, Pulford LJ, Fisher EM (2015) Dissecting Alzheimer disease in Down syndrome using mouse models. *Front Behav Neurosci* 9:268
126. Gardiner K, Fortna A, Bechtel L, Davisson MT (2003) Mouse models of Down syndrome: how useful can they be? Comparison of the gene content of human chromosome 21 with orthologous mouse genomic regions. *Gene*. 318:137–147
127. Gardiner KJ (2015) Pharmacological approaches to improving cognitive function in Down syndrome: current status and considerations. *Drug Des Devel Ther* 9:103–125
128. Rachidi M, Lopes C (2008) Mental retardation and associated neurological dysfunctions in Down syndrome: a consequence of dysregulation in critical chromosome 21 genes and associated molecular pathways. *Eur J Paediatr Neurol* 12:168–182
129. Rueda N, Florez J, Martinez-Cue C (2012) Mouse models of Down syndrome as a tool to unravel the causes of mental disabilities. *Neural Plast* 2012:584071

**Publisher's Note** Springer Nature remains neutral with regard to jurisdictional claims in published maps and institutional affiliations.